Science of the Total Environment 954 (2024) 176630

Contents lists available at ScienceDirect

Science of the Total Environment

journal homepage: www.elsevier.com/locate/scitotenv

Efficient microplastic identification by hyperspectral imaging: A comparative study of spatial resolutions, spectral ranges and classification models to define an optimal analytical protocol

Silvia Serranti *, Giuseppe Capobianco, Paola Cucuzza, Giuseppe Bonifazi

Department of Chemical Engineering, Materials & Environment, Sapienza University of Rome, Via Eudossiana 18, 00184 Rome, Italy

HIGHLIGHTS

- Hyperspectral imaging analytical protocols for efficient microplastics detection
- Comparative study of spatial resolutions, spectral ranges and classification models
- Definition of the detection limits for microplastics in different analytical setups
- Microplastics >250 μm can be identified with 150 μm/pixel in 1000–1700 nm by PLS-DA.
- Microplastics >100–200 μm can be identified with 30 μm/pixel in 1000–2500 nm by ECOC-SVM.

GRAPHICAL ABSTRACT

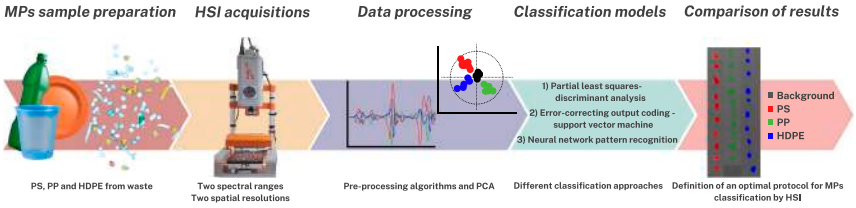

ARTICLE INFO

Editor: Bo Gao

Keywords:
Microplastic identification
Hyperspectral imaging
Chemometric analysis
Automatic classification
NIR-SWIR
Analytical protocol

ABSTRACT

Microplastics (MPs) pollution is a global and challenging issue, necessitating the development of efficient analytical strategies for their detection to monitor their environmental impact.

This study aims to define an optimal analytical protocol for characterizing MPs by hyperspectral imaging (HSI), comparing different setups based on spatial resolution, spectral range and classification models. The investigated MPs include polymers commonly found in the environment, such as polystyrene (PS), polypropylene (PP) and high-density polyethylene (HDPE), subdivided in three size classes (1000–2000 μm, 500–1000 μm, 250–500 μm). Furthermore, MP particles with diameters ranging from 30 to 250 μm were assessed to determine the limit of detection (LOD) in the different configurations. Hyperspectral images were acquired with two spatial resolutions, 150 and 30 μm/pixel, and two spectral ranges, 1000–1700 nm (NIR) and 1000–2500 nm (SWIR). Three classification models, Partial Least Square-Discriminant Analysis (PLS-DA), Error Correction Output Coding-Support Vector Machine (ECOC-SVM) and Neural Network Pattern Recognition (NNPR) were tested on the acquired images. The correctness of these models was evaluated by prediction maps and statistical parameters (Recall, Specificity and Accuracy). The results demonstrated that for MP particles larger than 250 μm, the optimal setup is a spatial resolution of 150 μm/pixel and a spectral range of 1000–1700 nm, utilizing a linear classification model like PLS-DA. This approach offers accurate predictions while being time- and cost-efficient. For MPs smaller than 250 μm, a higher spatial resolution of 30 μm/pixel with a spectral range of 1000–2500 nm and a non-linear classification method like ECOC-SVM is preferable. The LOD is 250 μm for the 150 μm/pixel

* Corresponding author.
E-mail address: silvia.serranti@uniroma1.it (S. Serranti).

https://doi.org/10.1016/j.scitotenv.2024.176630
Received 3 August 2024; Received in revised form 23 September 2024; Accepted 28 September 2024
Available online 2 October 2024

resolution and ranges from 100 to 200 μm for the 30 μm/pixel resolution. These findings provide a valuable guide for selecting the appropriate HSI acquisition conditions and data processing methods to optimally characterize MPs of different sizes.

1. Introduction

Microplastics (MPs) can be defined as plastic particles of primary or secondary origin ranging in size between 5.000 and 0.1 μm (Munoz-Pineiro, 2018). MPs pollution has significantly increased over the last century in many marine and terrestrial environments (Du et al., 2020; Hale et al., 2020; Issac and Kandasubramanian, 2021; Welsh et al., 2022; Cheung and Not, 2023; Christian and Köper, 2023; Rani-Borges et al., 2023), and they have even been detected in humans (Ragusa et al., 2021; Vethaak and Legler, 2021; Liu and You, 2023). For these reasons, global attention to MPs as an emerging ubiquitous pollutant is steadily growing and there is the need to find efficient, fast and accurate methods to detect and analyze these particles in different environmental matrices.

In recent years, several studies have been carried out on analytical techniques useful for detecting and quantifying MPs (Zarfl, 2019; Kavya et al., 2020; Yang et al., 2021; Du et al., 2022; Huang et al., 2023; Lee et al., 2023). However, the great variety in size, shape and composition of MPs still makes their recognition a very complex challenge. In this context, analytical methods that allow the identification of the type of polymer are an essential part of MPs studies.

In recent years, hyperspectral imaging (HSI) has emerged as a powerful technique for the analysis of MPs in environmental samples (Serranti et al., 2018; Serranti et al., 2019; Faltynkova et al., 2021; Fiore et al., 2022; Faltynkova and Wagner, 2023). This advanced sensing technique combines the spatial information of digital imaging with the spectral information of spectroscopy, collecting a spectral signature for every pixel of the acquired image in the investigated wavelength range with a high spectral resolution. The acquired three-dimensional datasets are usually called hypercubes and they are processed in order to extract the required information by chemometric logics (Datta et al., 2022; Ozdemir and Polat, 2020; Calvini et al., 2019; Gewali et al., 2018; Amigo et al., 2013).

HSI working in the NIR-SWIR regions (1000–1700 and 1000–2500 nm) has been successfully applied to identify plastic waste by polymer in the recycling industry (Bonifazi et al., 2023; Cucuzza et al., 2023). This proven capability can be transferred to address the growing challenge of microplastic analysis, thanks to the flexibility of HSI to be applied from macro- to micro- scale, modifying field of view and pixel resolution, according to the size of the analyzed samples (Faltynkova et al., 2021; Vidal and Pasquini, 2021; Shan et al., 2019; Schmidt et al., 2018). In addition, HSI technique is highly attractive due to its minimal sample preparation required for MPs acquisition. Despite the great advantages of HSI in MPs identification, especially in the reduction of analysis time in comparison with the most popular techniques usually applied, such as FT-IR and Raman spectroscopy, there is the need to define a standardized protocol for MPs analysis by HSI. The main aspects that must be better investigated for the definition of a standardized methodology are the appropriate selection of: 1) spatial resolution (i.e.: image pixel size); 2) spectral range and 3) classification model for data processing.

Spatial resolution in hyperspectral imaging systems refers to the sensor's ability to distinguish spatial details in the acquired image. It is determined by the size of the pixels in the sensor, affecting the sharpness and detail of images (Lodhi et al., 2019). The higher the spatial resolution, the smaller the details that can be resolved. However, increasing the spatial resolution often reduces the spectral resolution or sensitivity of the sensor. Higher spatial resolution means that the energy detected by each pixel is distributed over a smaller area, which can reduce the signal-to-noise ratio and therefore image quality (Chen et al., 2023). The selection of the spatial resolution of the HSI device is essential for the definition of the MPs particle limit of detection (LOD), ensuring that the system is optimized for detecting the smallest possible particles, facilitating at the same time the comparison of results across different studies. It is important to highlight that usually the spatial resolution does not coincide with the LOD as a particle can require more than just one pixel to provide a significant spectral signature (Faltynkova et al., 2021).

The choice of the spectral range is important both from an economic and technical point of view. A HSI sensor working in the spectral range of 1000–1700 nm is less expensive and is widely used for plastic recognition in various sectors. However, expanding the spectral range up to 2500 nm can significantly improve plastic recognition, particularly when the signal-to-noise ratio is low (Tasseron et al., 2021). Evaluating and comparing the results obtained in the identification of MPs by HSI working in NIR and SWIR ranges, respectively, can allow to assess the capability to distinguish between different polymers in the two spectral ranges, based on their typical spectral signatures, also determining the LOD of MPs particles in each spectral range. Based on the results, it could be possible to define if the wavelength range of 1700–2500 nm must be included for the optimal classification and to select the most cost-effective solution according to the investigated MPs samples.

Finally, the selection of the most appropriate classification model is a crucial aspect for material recognition by HSI. Linear models, such as partial least squares-discriminant analysis (PLS-DA), are simple, quick to train, and easy to interpret. However, they are limited in handling the complexities of hyperspectral data, where relationships between variables can be nonlinear. Nonlinear models, such as nonlinear support vector machines or neural networks, offer greater flexibility in capturing these complexities and improve recognition accuracy (Cao et al., 2017). However, the training process can be more complex in nonlinear models and increases the risk of overfitting if the hyperspectral data have a linear trend. The comparison of different classification models for data processing can help to identify which model provides the most reliable results according to the size of MPs particles, finding a balance between computational complexity and accuracy and reducing in this way the analysis time.

The primary objective of this study is therefore to investigate the above-mentioned aspects in order to define a valuable protocol for the characterization of MPs by HSI, as a rapid, non-invasive and non-destructive analytical method. This protocol aims to provide valuable information on HSI-based analytical procedure to improve computational and instrumental efficiency in MPs identification of different sizes. MPs classification results obtained by different HSI-based analytical setups are compared and discussed, with reference to the selection of two different spatial resolutions and spectral ranges and three classification models, whose efficiency was evaluated in terms of prediction maps and statistical parameters (Recall, Specificity and Accuracy). Finally, a LOD analysis for the different setups was carried out, defining the optimal analytical conditions for MPs particles ranging from 30 to 250 μm.

2. Materials and methods

2.1. Microplastic samples preparation

The studied MPs samples were obtained from the comminution of post-consumer plastic packaging selected among the most widespread polymers in the environment, such as PS, PP and HDPE (Duis et al., 2016; Rytelewska et al., 2022). Size reduction process was performed using a cutting mill (SM 2000, Retsch GmbH, Germany). For each studied polymer, 3 size classes were prepared using stacked sieves, i.e.,

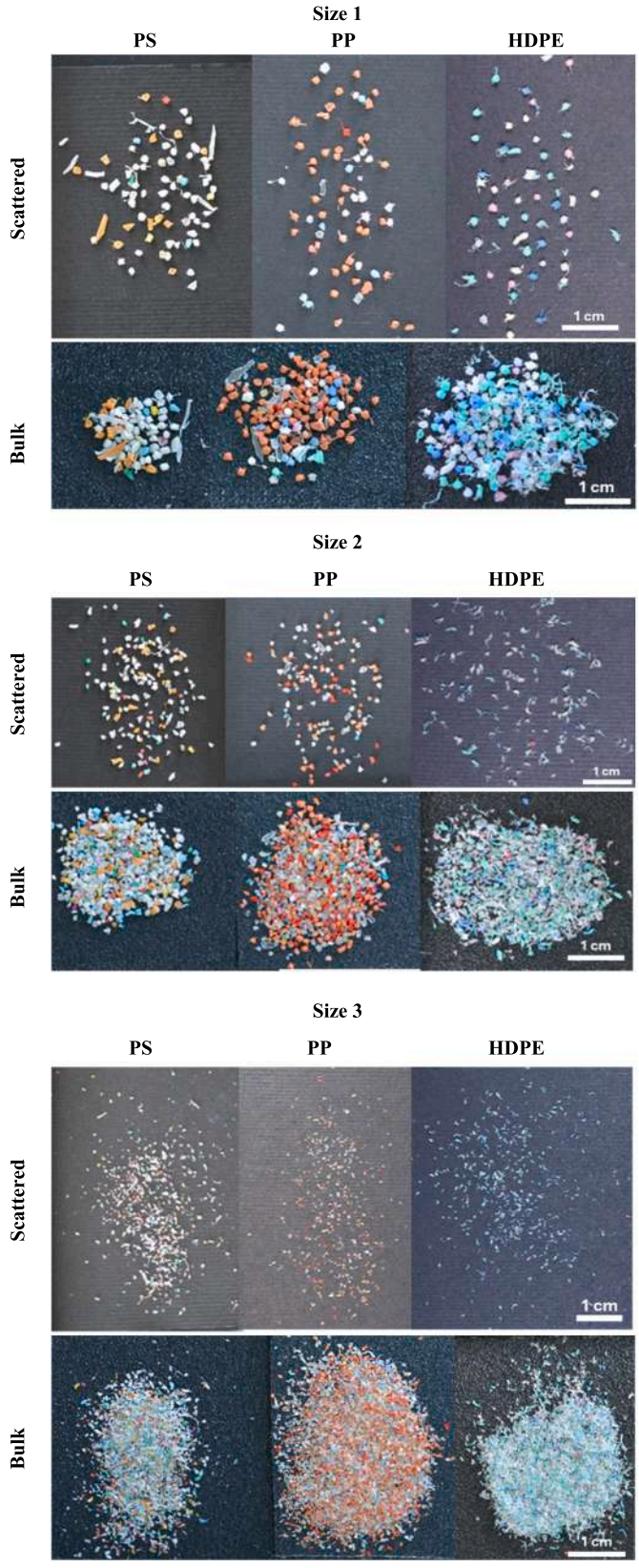

(a)

Fig. 1. Selected MPs of the three polymers (PS, PP and HDPE) for each size class (isize 1: −2000 μm +1000 μm; size 2: −1000 μm +500 μm; size 3: −500 μm +250 μm) disposed on a black background both scattered and bulk to build the calibration dataset (a) and disposed in line to create the validation dataset (b).

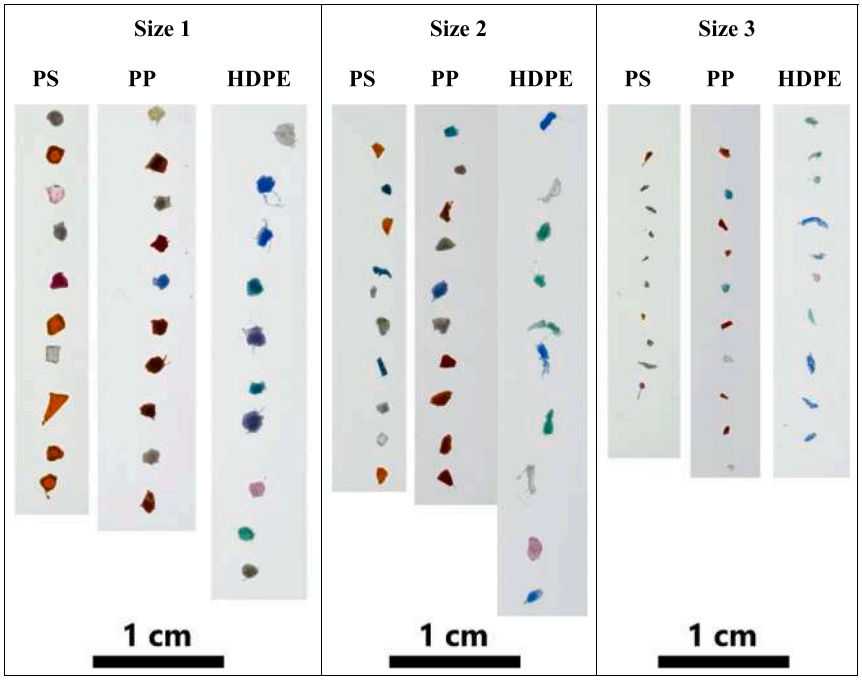

(b)

Fig. 1. (*continued*).

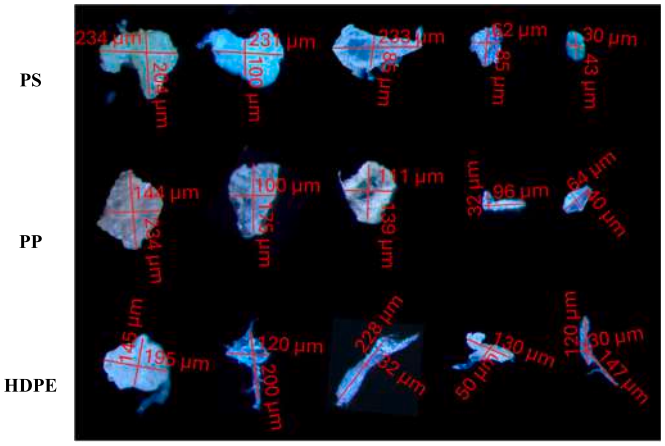

Fig. 2. Selected MPs of the three polymers with diameters ranging from about 30 to 250 μm used for the LOD evaluation.

size 1: −2000 μm +1000 μm; size 2: −1000 μm +500 μm; size 3: −500 μm + 250 μm. Selected MPs particles of the three polymers for each size class were disposed on a black background both scattered and bulk to build the calibration dataset (Fig. 1a) and in line (Fig. 1b) to build the validation dataset, enhancing discrimination capabilities of the smallest particles and considering the variance related to their three-dimensional nature and signal disturbances arising from particle proximity.

Furthermore, MPs particles with a diameter from 30 to 250 μm were selected under a stereomicroscope (Fig. 2) to evaluate the LOD for the different HSI architecture set-up (in terms of investigated spectral range, spatial resolution and classification model).

2.2. Analytical methods

2.2.1. Hyperspectral imaging architecture setups

Image acquisitions were carried out using the pushbroom sensor "Sisuchema XL™ Chemical Imaging Workstation", embedding an ImSpector™ N25E (Specim®, Finland), operating in the SWIR range (1000–2500 nm), coupled with a MCT camera (320 × 240 pixels) and located at the Raw Materials Laboratory (RawMaLab) of the Department of Chemical Engineering, Materials & Environment (DICMA) of Sapienza University of Rome. The number of acquired spectral bands is 240, with a spectral resolution of 10 nm. Hyperspectral images were acquired at two different spatial resolutions, using two different objectives: 1) a 31 mm lens, covering a 5 cm field of view (FOV) corresponding to a spatial resolution of 150 μm/pixel and a scanning speed of 17.35 mm/s; 2) a macro lens, covering a 1 cm FOV, corresponding to a spatial resolution of 30 μm/pixel and a scanning speed of 2.55 mm/s. A diffused line-illumination unit was adopted optimizing the imaging of various surfaces. Reflectance of hypercubes is automatically set up by an internal standard reference target.

2.2.2. Hyperspectral data handling and analysis

Different hyperspectral images of MPs, including PS, PP and HDPE particles, considering the three investigated size classes (size 1, 2 and 3), were acquired at two different spatial resolutions (i.e., 150 μm/pixel and 30 μm/pixel, respectively), with two different particle grouping, i.e. scattered and bulk, in order to create the calibration and validation datasets. The datasets were acquired in the spectral range 1000–2500 nm and they were then reduced to obtain the range 1000–1700 nm, resulting in distinct datasets for each of the two spectral ranges.

Two mosaic calibration datasets (Fig. S1) were generated, one for each spatial resolution, comprising 18 hyperspectral images (i.e. 3 polymers × 3 size classes x 2 different particle grouping). The dimensions of the mosaic calibration dataset acquired at 150 μm/pixel are 710 × 2611 pixels with a size of 3.8 GB for the dataset in the range 1000–2500 nm and 1.7 GB for the dataset in the range 1000–1700 nm. The dimensions of the mosaic calibration dataset acquired at 150 μm/pixel are 2017 × 2880 pixels with a size of 11.95 GB for the dataset in the range 1000–2500 nm and 5.3 GB for the dataset in the range 1000–1700 nm.

Furthermore, a mosaic validation dataset was created consisting of 9

hyperspectral images (i.e.: 3 polymers × 3 size classes), for both the spatial resolutions, containing selected MP particles disposed in line and employed to evaluate the prediction performances of the classifiers in identifying MPs of different sizes. The dimensions of the mosaic validation dataset acquired at 150 μm/pixel are 748 × 367 pixels with a size of 544.5 MB for the dataset in the range 1000–2500 nm and 242.96 MB for the dataset in the range 1000–1700 nm. The dimensions of the mosaic validation dataset acquired at 30 μm/pixel are 1597 × 1491 pixels with a size of 4.9 GB for the dataset in the range 1000–2500 nm and 2.2 GB for the dataset in the range 1000–1700 nm.

Finally, to evaluate the LOD of MP particles, a specific test was carried out on individual particles with size ranging from 30 to 250 μm. These particles were classified applying all the developed models in the two considered spatial resolutions and spectral ranges.

The HSI data processing was carried out using different tools running inside MATLAB® environment (version R2022b, The Mathworks, Inc., Natick, MA, USA), namely: PLS toolbox (ver. 9.2 Eigenvector Research, Inc., Wenatchee, WA, USA) for PCA and PLS-DA, and Statistics and Machine Learning Toolbox™ for ECOC-SVM and NNPR.

2.2.2.1. Image pre-processing. The pre-processing algorithms were chosen among those most applied to NIR data (Rinnan et al., 2009; Esquerre et al., 2012; Vidal and Amigo, 2012; Amigo et al., 2015), including those related to plastic samples (Serranti et al., 2012; Vidal et al., 2012; Serranti et al., 2020; Bonifazi et al., 2022). In particular, the combination of Standard Normal Variate (SNV) (Barnes et al., 1989), 1st Derivative (Savitzky and Golay, 1964) (window of 15 points) and Mean Center (MC) (Jolliffe, 1986) was used to highlight the spectral differences between the studied classes of polymers and to remove anomalous values. SNV allows to solve scaling or gain effect due to path length and scattering effects, detector changes, or other instrumental sensitivity effects. Derivative is an algorithm used to remove insignificant baseline signal from data. MC was used to center the data, in fact it is a method used to eliminate the data offset which is not of interest for the variance data interpretation (Bro and Smilde, 2003; Amigo et al., 2015).

2.2.2.2. Principal Component Analysis (PCA). PCA was utilized with explorative purposes and to evaluate the best pre-processing strategy according to the separation in the score plots of the considered classes (i.e., Background, PS, PP and HDPE) and to reduce the dimensionality of the data in the ECOC-SVM and NNPR classifiers. PCA is an unsupervised method that allows compression of the data dimensionality at the same time reducing to a minimum the loss of information, projecting samples into a lower dimensional subspace where the axes, called Principal Components (PCs), point in the maximal variance direction. The loading vectors, which are the coefficients of the original variables in each principal component, indicate the contribution of each feature to the PCs and thus help in understanding the underlying structure of the data. Looking at the PCA score plot, it is possible to detect similarities among samples: the more they are grouped, the more they have similar spectral behavior (Jolliffe, 2002; Amigo et al., 2013; Bro and Smilde, 2014).

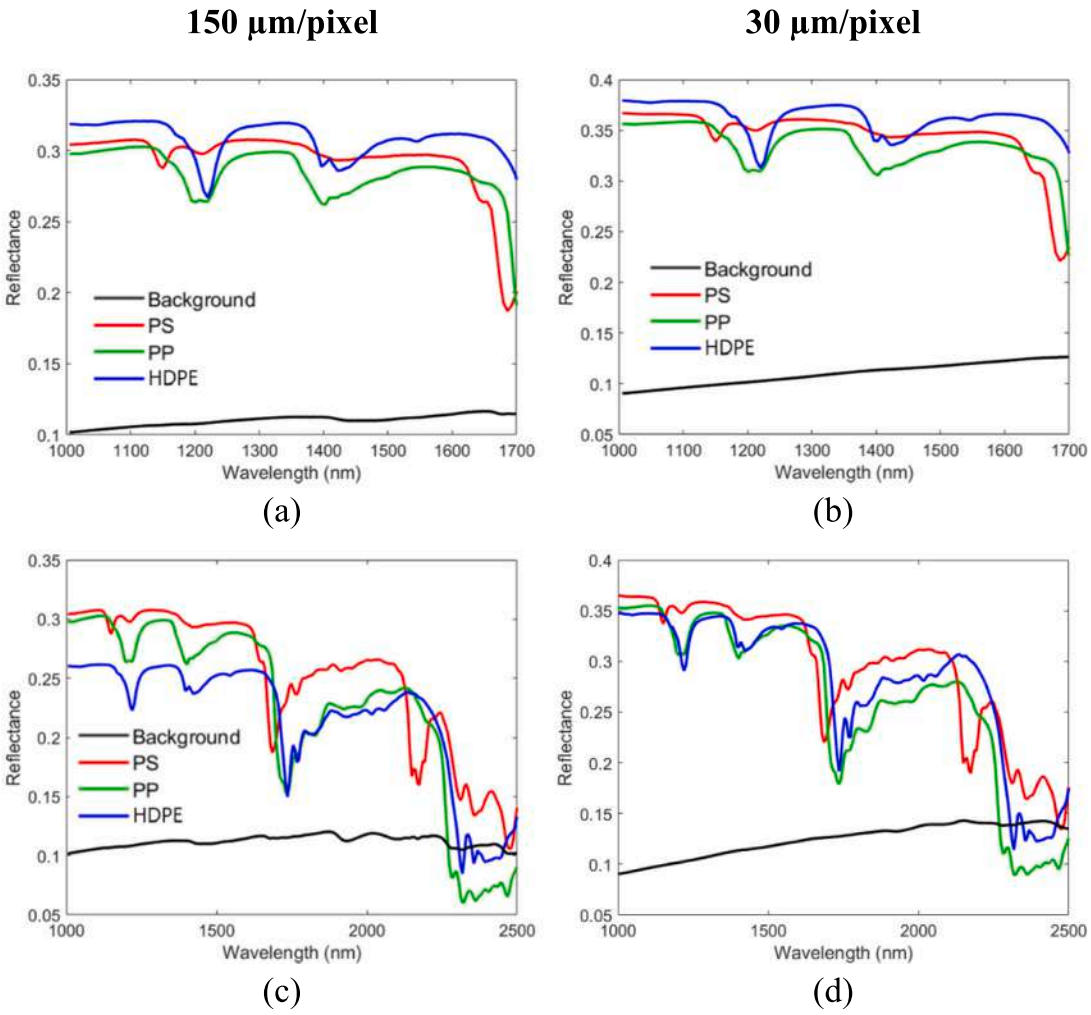

Fig. 3. Average raw reflectance spectra in the 1000–1700 nm spectral range of the calibration dataset at 150 μm/pixel resolution (a) and at 30 μm/pixel resolution (b); average raw reflectance spectra in the 1000–2500 nm spectral range of the calibration dataset at 150 μm/pixel resolution (c) and at 30 μm/pixel resolution (d).

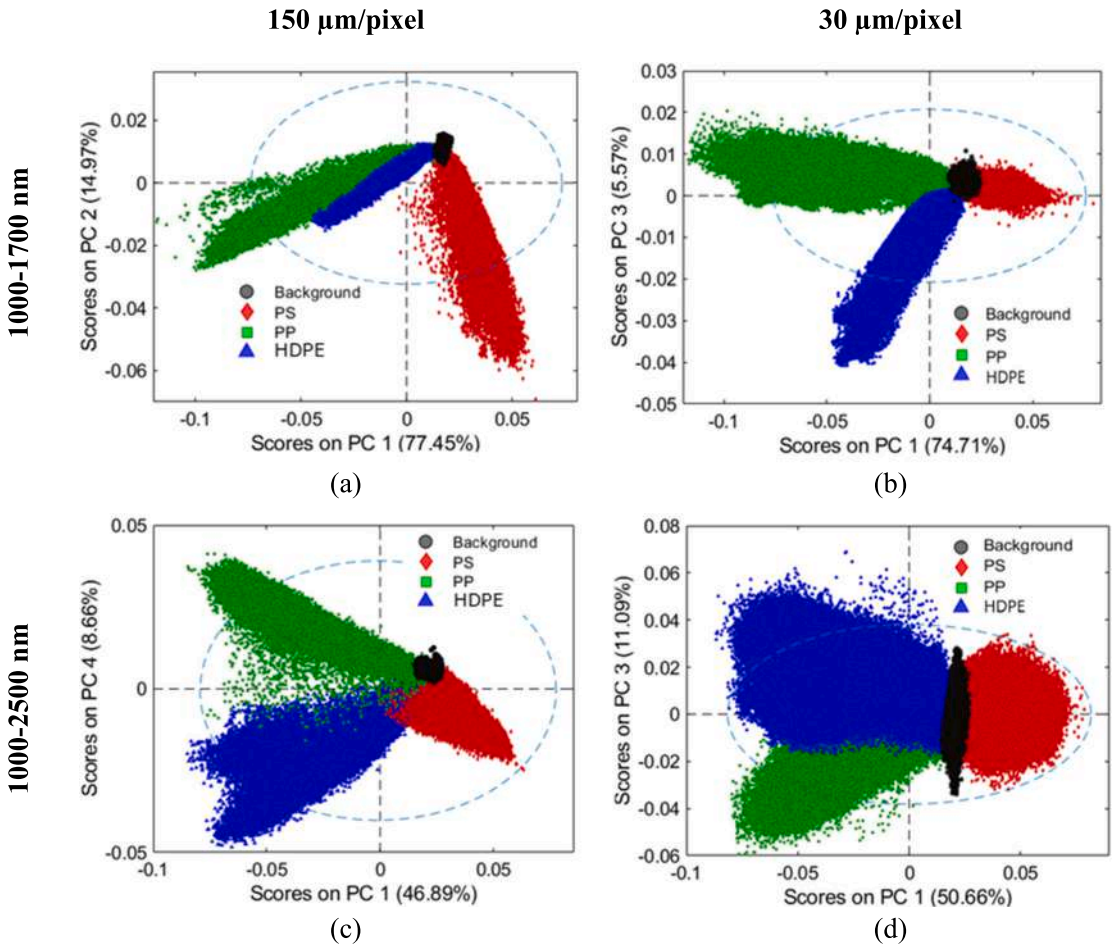

Fig. 4. PCA score plots of calibration data in the spectral range from 1000 to 1700 nm at 150 µm/pixel resolution (a) and 30 µm/pixel resolution (b), PCA score plots of calibration data in the spectral range from 1000 to 2500 nm at 150 µm/pixel resolution (c) and at 30 µm/pixel resolution (d).

2.2.2.3. Classification models. Three types of four-class (Background, PS, PP and HDPE) classification models were selected, characterized by different data processing and approaches: PLS-DA, ECOC-SVM and NNPR. In detail, PLS-DA was selected as the most common classification model based on data covariance (Ballabio and Consonni, 2013). PLS-DA is a supervised method that needs prior knowledge of the data to classify samples into predefined and known classes (Barker and Rayens, 2003; Ballabio and Consonni, 2013). It is a classification method that combines the partial least squares regression features with the discriminant ability. In order to evaluate the model complexity and choose the appropriate number of Latent Variables (LVs), each PLS-DA model was cross-validated using the Contiguous block method. ECOC-SVM was selected because it has the benefit of non-linearly mapping the sample to the higher dimensional space for dealing with a non-linear relationship between observation and classes (Mishra et al., 2018). ECOC-SVM is a classification method composed by two parts. The first part, called "ECOC", represents a coding method that treats each binary classification model as a transmission channel and converts samples through the output codes to their correct categories allowing to convert multi-class problems into multiple binary problems. The second part, named "SVM", represents the binary classification that creates boundaries between sample responses to provide a class region based on classification functions generated from the information available for each sample. These functions and boundaries can then predict new samples (Deng et al., 2017; Duan et al., 2021). Finally, NNPR was selected as one of deep learning-based methods that achieves promising performances with high-dimensional data, such as hyperspectral images (Hu et al., 2015). NNPR is a novel research direction in the field of pattern recognition, it has many advantages compared to the traditional pattern recognition methods, such as robustness, efficient fault-tolerant and self-learning (Zhou et al., 2016). Generally, a complete NNPR architecture is divided into three layers, namely, input, hidden and output layers. These neurons are connected by links with weights that are selected to meet the expected relationship between input and output neurons (Li et al., 2014; Chang et al., 2013). Here the customized network of "*Patternnet*" in Matlab was used, solving the pattern recognition problem using two-level feed-forward networks. For the weight initialization, the Nguyen-Widrow initialization algorithm was used. The activation function and training algorithm for feed-forward were the tangent sigmoid and Levenberg-Marquardt method, respectively. For the NNPR model, dimensionality reduction through PCA reduced sensitivity to variations in hyperparameters, such as the number of neurons and the learning rate, thus simplifying its construction and decreasing computational load. To optimize hyperparameters, the calibration dataset was split into 70 % for training and 30 % for validation. Model performance was evaluated using the cross-entropy error, which measures the difference between predicted probabilities and actual class probabilities, with a layer size set to 30. Finally, the model was validated on an external dataset, using the same approach as for PLS-DA and ECOC-SVM.

2.2.2.4. Performance metrics. In a 4-class classification model, True Positives (TP), True Negatives (TN), False Positives (FP) and False Negatives (FN) are calculated for each class by treating one class as positive and all others as negative. TP refers to instances correctly classified in the current class, TN are instances that belong to other classes and are correctly excluded from the current class, FP are

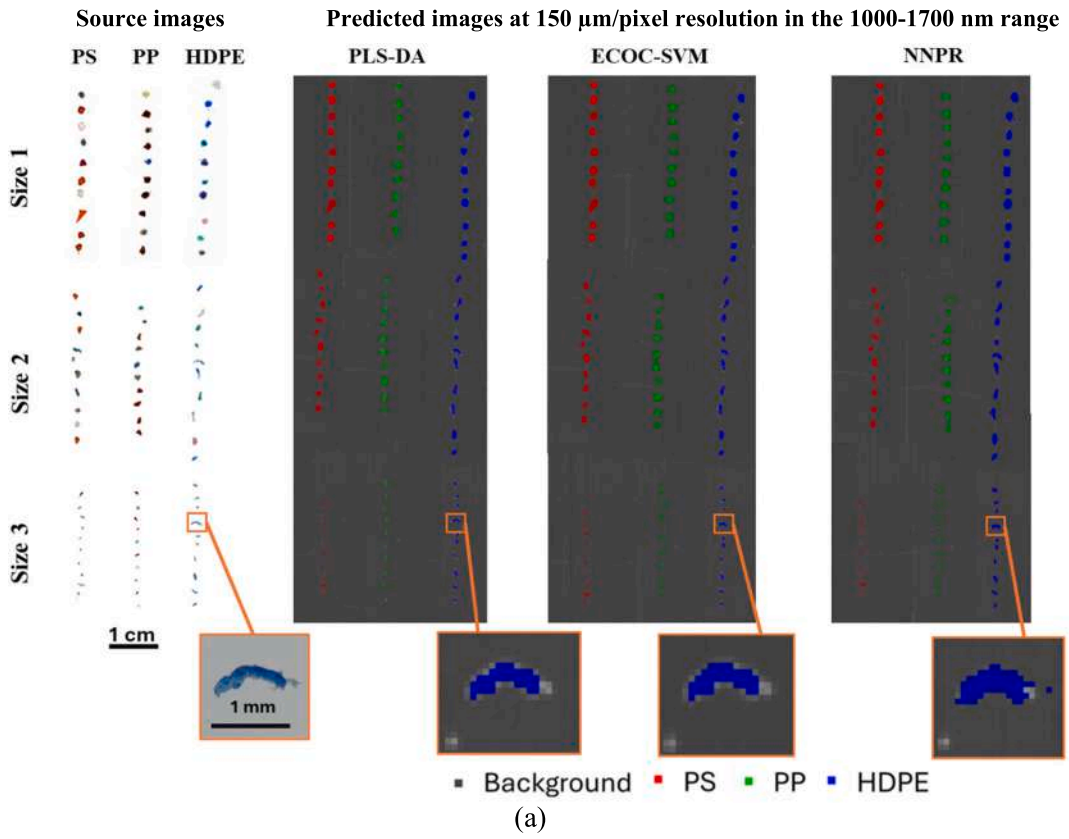

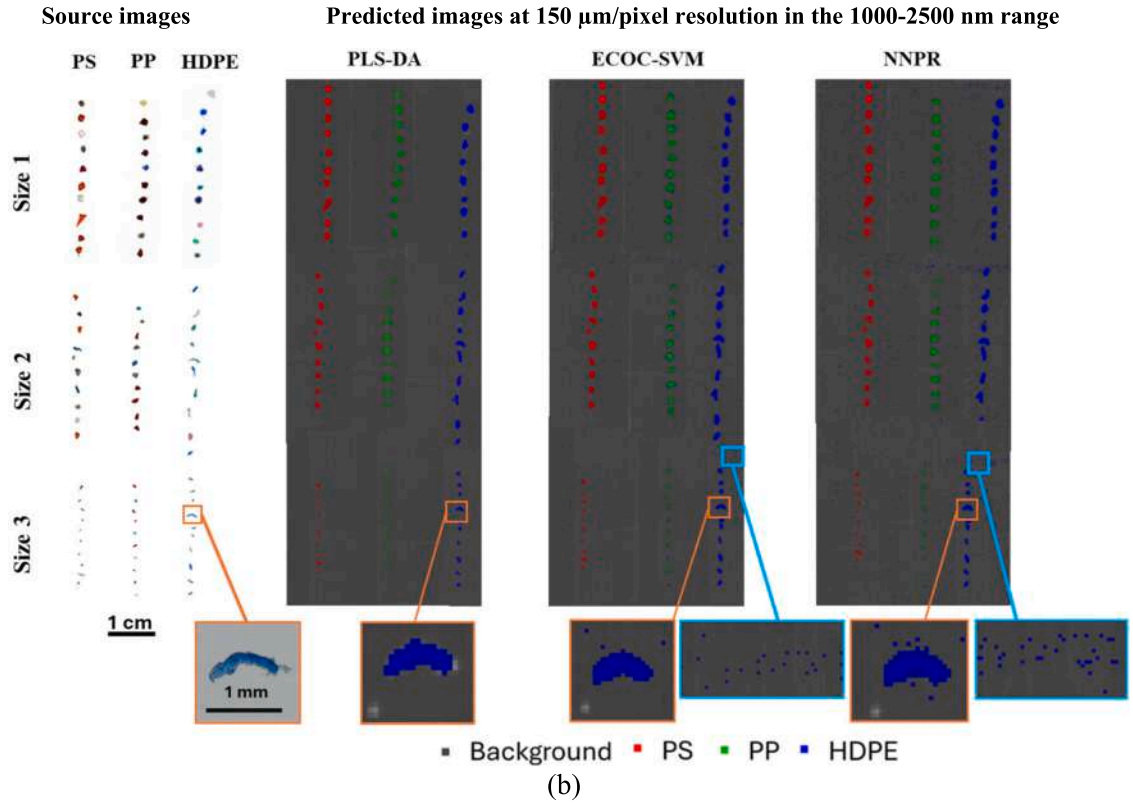

Fig. 5. Predicted images of the validation dataset at 150 µm/pixel resolution, in the spectral ranges of 1000–1700 nm (a) and (b) 1000–2500 nm, obtained by PLS-DA, ECOC-SVM and NNPR. The colored boxes highlight detailed results for each classifier, useful for comparing the misclassification errors among them.

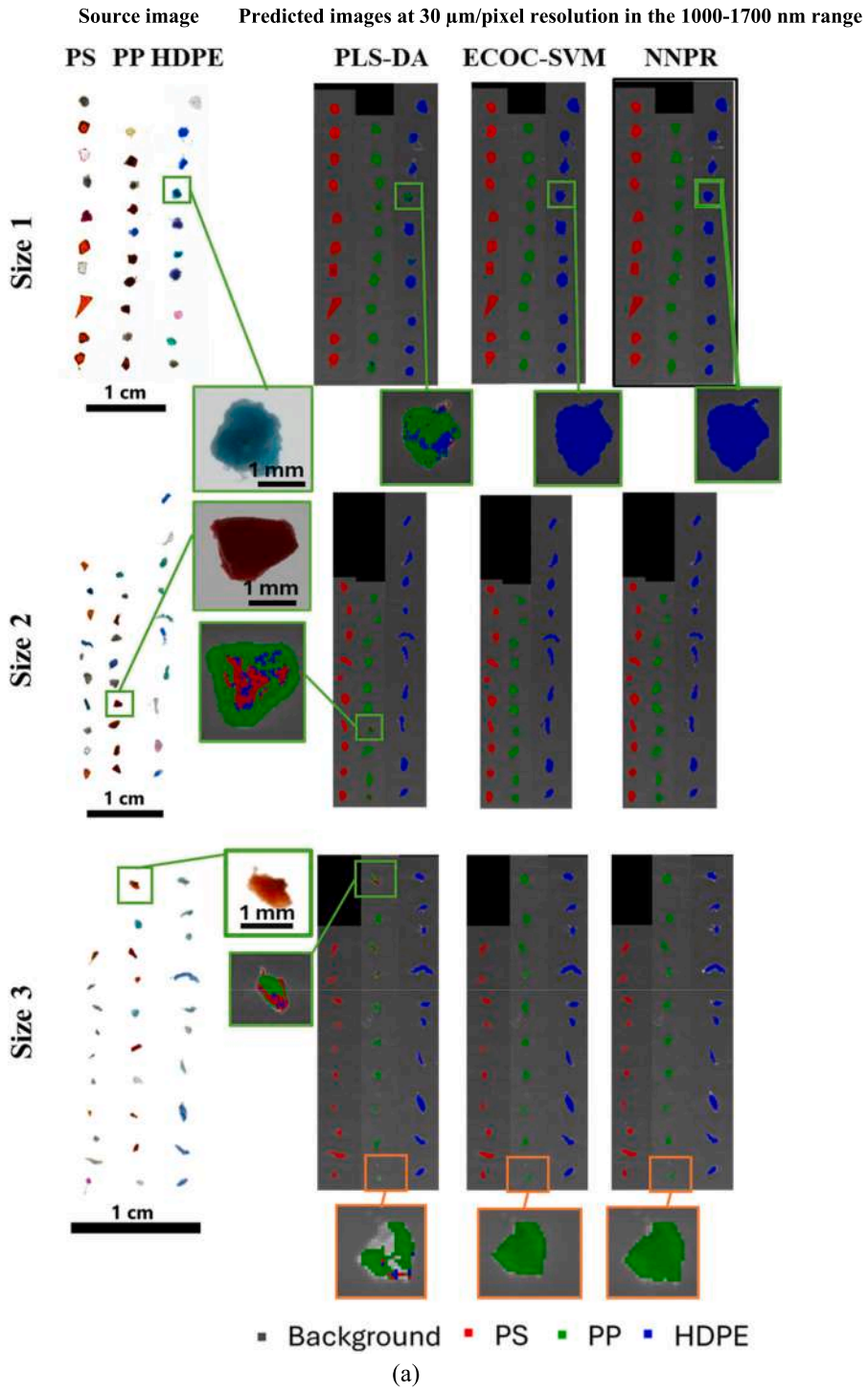

(a)

Fig. 6. Predicted images of the validation dataset at 30 µm/pixel resolution, in the spectral ranges of 1000–1700 (a) and 1000–2500 nm (b), obtained by PLS-DA, ECOC-SVM and NNPR. The colored boxes highlight detailed results for each classifier, useful for comparing the misclassification errors among the three classifiers.

instances from other classes incorrectly classified as belonging to the current class and FN are instances of the current class incorrectly classified as belonging to other classes. From the values of TP, TN, FP and FN, Recall (or Sensitivity in binary classification), Specificity, and Accuracy can be derived. Recall is defined as the number TP divided by the sum of TP and FN. Specificity is the number of TN divided by the sum of TN and FP. Accuracy is the proportion of correctly classified instances (both TP and TN) relative to the total number of instances (TP, TN, FP, FN), representing the overall effectiveness of the classification model (Eigenvector, 2018). These metrics range from 0 to 1, with 1 indicating the ideal value. The parametric performance of each developed classification model was calculated using a pixel-based approach, considering calibration (Cal) and cross-validation (CV) for the training set, as well as prediction (Pred) for the validation set.

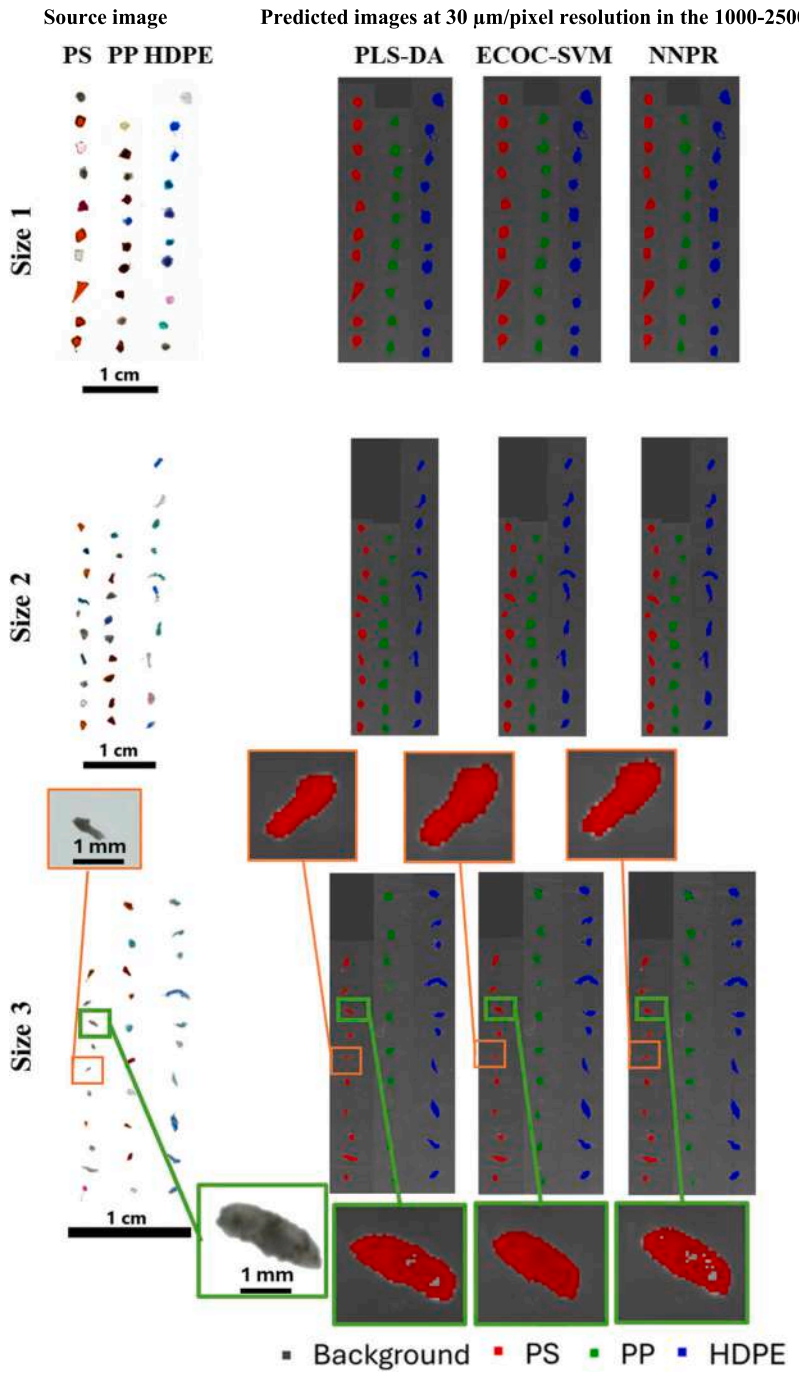

(b)

Fig. 6. (*continued*).

3. Results and discussion

3.1. Datasets spectral features and PCA results

The average raw reflectance spectra of the studied classes (i.e. Background, PS, PP and HDPE) in the spectral range 1000–1700 and 1000–2500 nm of the calibration dataset at 150 µm/pixel and 30 µm/pixel (Fig. 3a-b and c-d, respectively) show very low differences, mainly related to the reflectance levels.

The spectra of PP and HDPE from 1000 to 1700 nm range are mainly characterized by aromatic C—H and C—H_2 stretch of the third and second overtone, while extending the range until 2500 nm it is possible to obtain the information regarding C—H bending and C—H stretch in the first combination region (Miller, 1991; Workman and Weyer, 2012; Bonifazi et al., 2018; Bonifazi et al., 2023; Beć et al., 2021). PS spectrum from 1000 to 1700 nm range is mainly characterized by C—H_2 stretch and C—H_2 deformation of third and second overtone, while extending the range until 2500 nm it is possible to obtain the information regarding aromatic C—H stretch plus C—H bending of first overtone and aromatic C—H stretch plus sum band (Miller, 1991; Weyer, 2007; Workman and Weyer, 2012; Beć et al., 2021). The black background shows a low and flat reflectance signal in both the investigated wavelength ranges. All these spectral characteristics are emphasized in the pre-processed spectra for both magnifications and spectral ranges, as

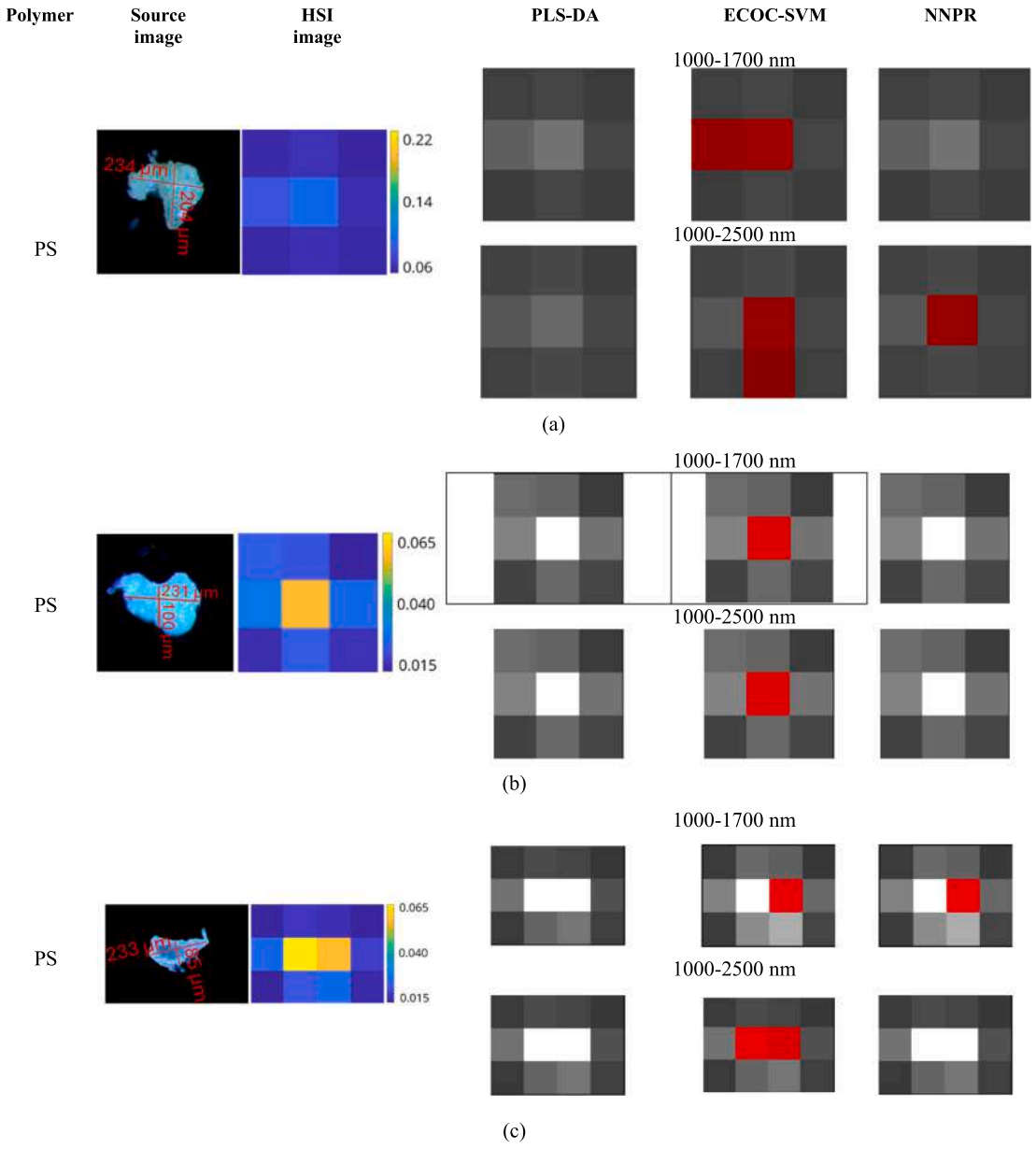

Fig. 7. Source image, hyperspectral image with reflectance color bar and classification results of PLS-DA, ECOC-SVM and NNPR models applied to hyperspectral images of MP particles (PS, PP and HDPE) at resolution of 150 μm/pixel in the 1000–1700 and 1000–2500 nm spectral ranges.

shown in Fig. S2.

Fig. 4 shows the PCA score plots for the four calibration datasets (i.e.: 150 μm/pixel and 1000–1700 nm (Fig. 4a), 30 μm/pixel and 1000–1700 nm (Fig. 4b), 150 μm/pixel and 1000–2500 nm (Fig. 4c) and 30 μm/pixel and 1000–2500 nm (Fig. 4d), highlighting the principal components that allow the best separation between polymer classes. The PCA score plots demonstrate how the selected preprocessing methods allow for good separation of the microplastics from the background in all four calibration datasets, with four clusters of points corresponding to the four considered classes (Background, PS, PP and HDPE). Further details regarding the PCA score and loading plots are provided in the supplementary materials under the section "PCA score and loading plots results" and Fig. S3.

3.2. Classification results

The predictive results of the classifiers PLS-DA, ECOC-SVM and NNPR, applied to the validation dataset at spatial resolutions of 150 and 30 μm/pixel, in the 1000–1700 and 1000–2500 nm spectral ranges, are reported and discussed in the following.

3.2.1. 150 μm/pixel resolution

The prediction maps at 150 μm/pixel resolution (Fig. 5a and b) show as all MPs of different sizes are assigned to the correct polymer class. However, some misclassification errors occur between particle edges and background. Considering the 1000–1700 nm range, in the orange boxes of Fig. 5a it is highlighted, for all the classifiers, the wrong assignment of background pixels along the edge of a HDPE particle from size class 3, however it does not reduce the effectiveness of microplastics recognition. Furthermore, considering the 1000–2500 nm range (Fig. 5b), it can be observed how ECOC-SVM and NNPR not only misclassify pixels along the edge of the HDPE particle (orange boxes), but there is also a "salt&pepper noise" (light blue boxes) in the background due to the wrong assignment of some pixels to the HDPE class.

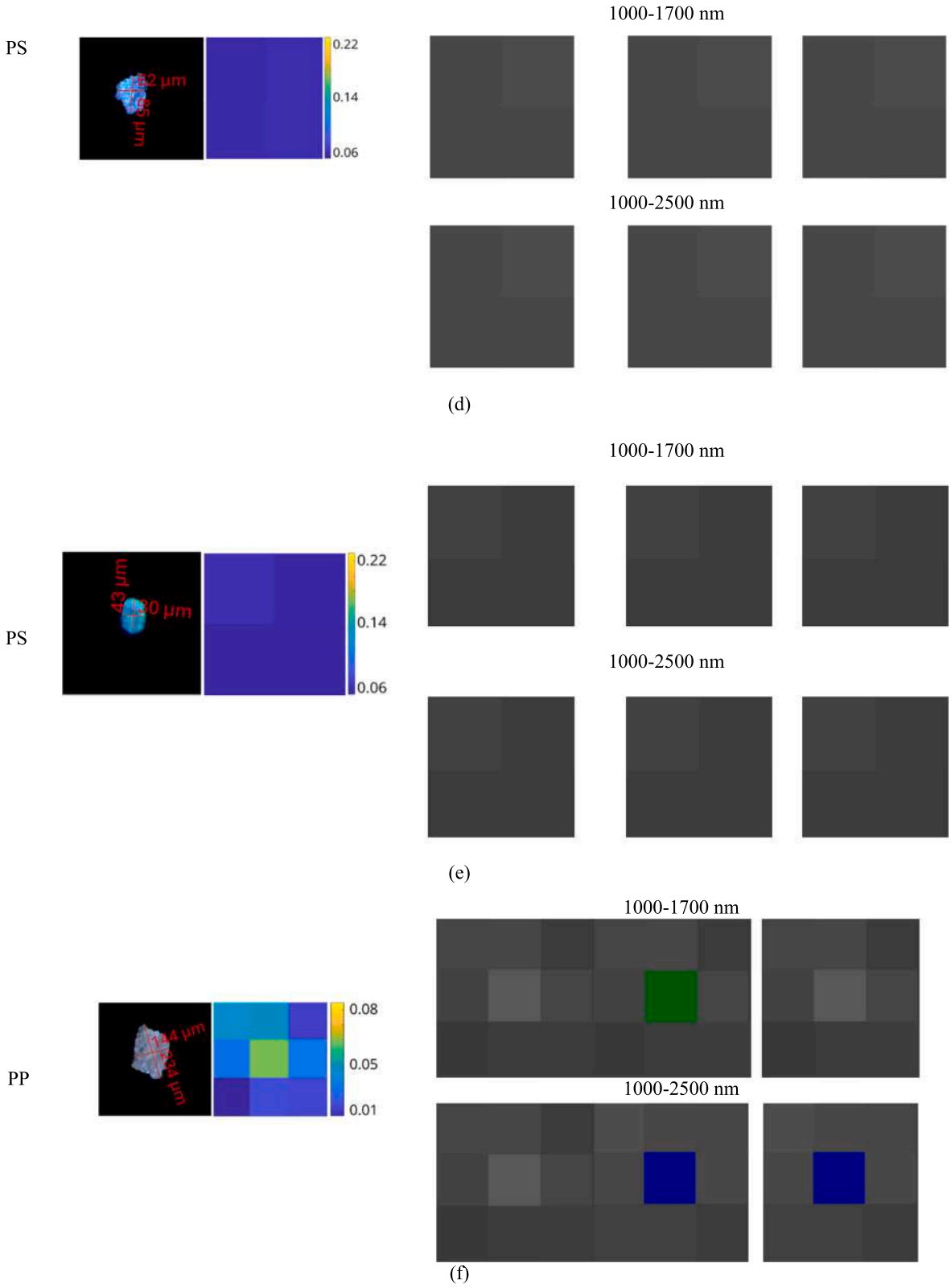

Fig. 7. (*continued*).

On the contrary, PLS-DA shows a better recognition of background and polymer classes.

The performance parameters Recall, Specificity and Accuracy in Cal and CV (Tables S1 and S2, respectively) highlight the robustness of all models: in the 1000–1700 nm spectral range, values range from 0.92 to 1.00 for PLS-DA, from 0.98 to 1.00 for ECOC-SVM and from 0.95 to 1.00 for NNPR, whereas in the 1000–2500 nm spectral range there are similar results, with values ranging from 0.91 to 1.00 for PLS-DA and from 0.97 to 1.00 for both ECOC-SVM and NNPR. The latter two models show slightly better performance in the calibration phase compared to PLS-DA

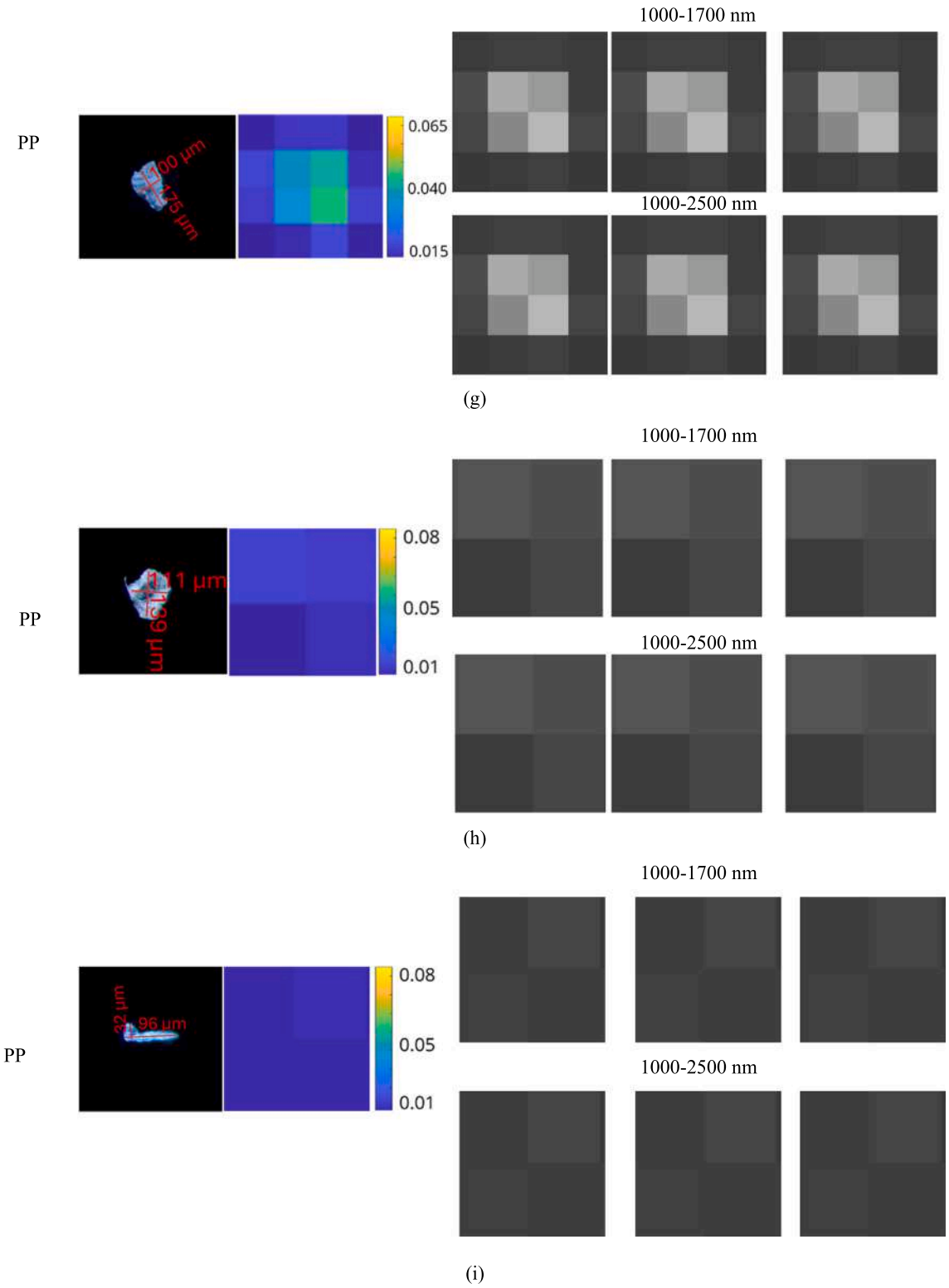

Fig. 7. (*continued*).

due to their ability to find complex and non-linear relationships in the data. The performances in prediction (Tables S3 and S4) agree with the results shown in the prediction images, in fact similar values were reached by the three classifiers in the 1000–1700 nm range (PLS-DA: from 0.76 to 1.00; ECOC-SVM: from 0.79 to 1.00 and NNPR: from 0.89 to 1.00), whereas in the 1000–2500 nm spectral range, PLS-DA provides the best performances (from 0.98 to 1.00) compared to ECOC-SVM (from 0.72 to 1.00) and NNPR (from 0.63 to 1.00). The latter result can be explained considering that hyperspectral images of MPs acquired at that spatial resolution are less influenced by the depth of field (DOF), allowing to obtain an accurate prediction with a linear classifier, like PLS-DA.

These results suggest that, at 150 μm/pixel resolution, using the 1000–1700 nm spectral range combined with the PLS-DA model offers a

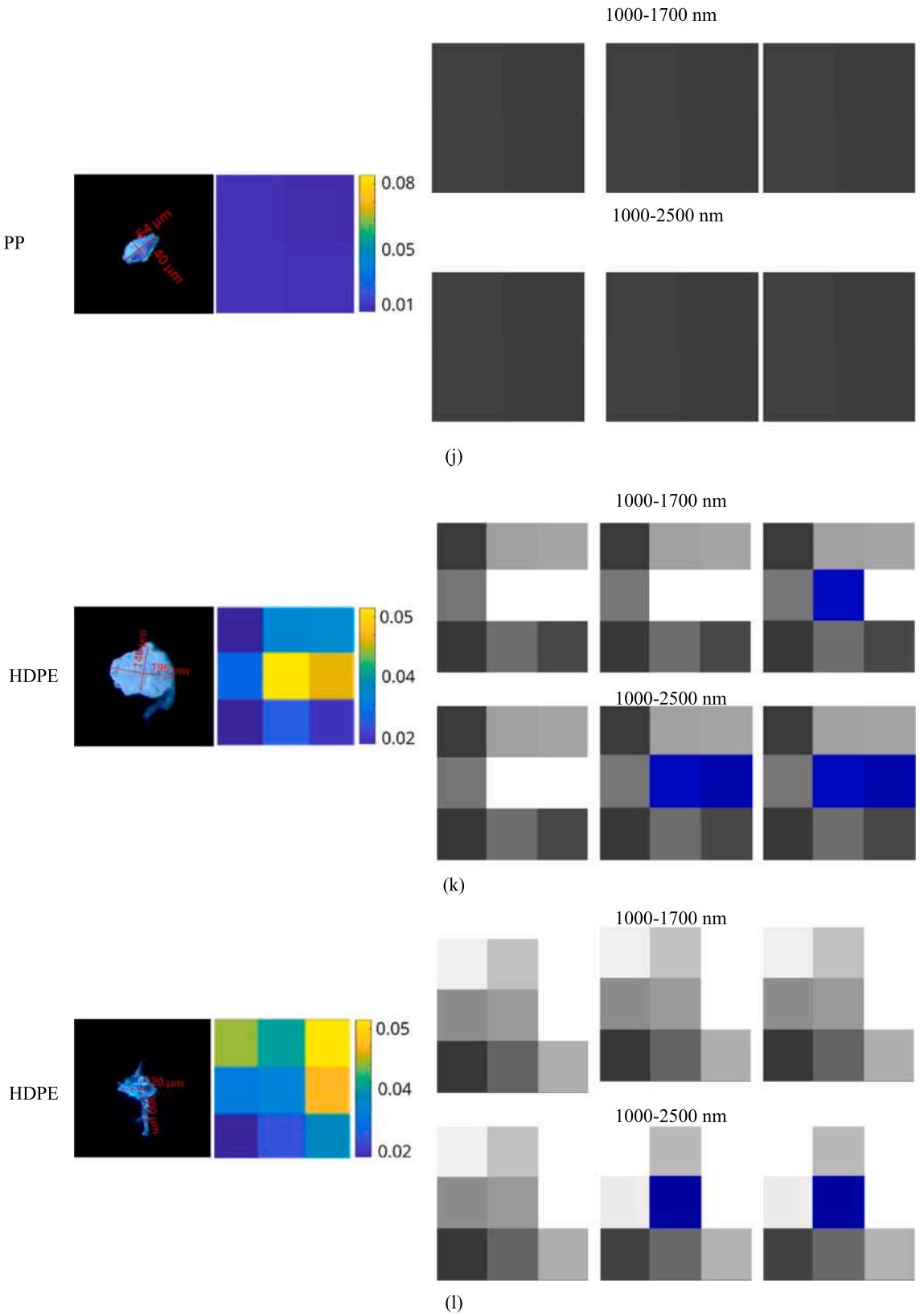

Fig. 7. (*continued*).

cost and time efficient method for MPs classification, delivering high accuracy while being easier and faster to apply than the two nonlinear models. The obtained results agree with those of other studies (i.e.: Zhu et al., 2020), which successfully utilized a HSI system in the range 1000–1700 nm to classify MPs, allowing to reduce costs and simplify data processing in comparison to the range 1000–2500 nm, as suggested by Faltynkova et al. (2021).

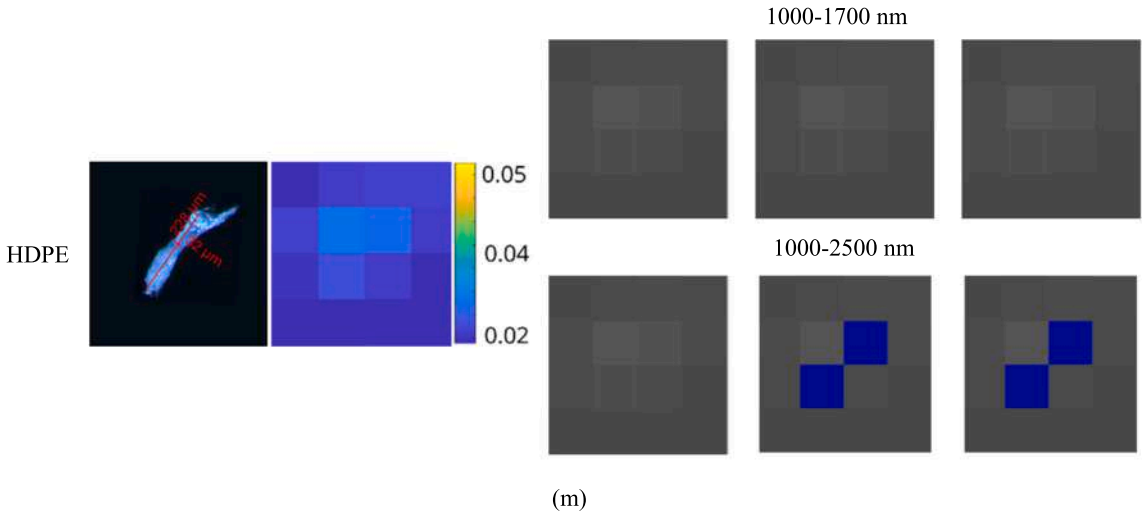

(m)

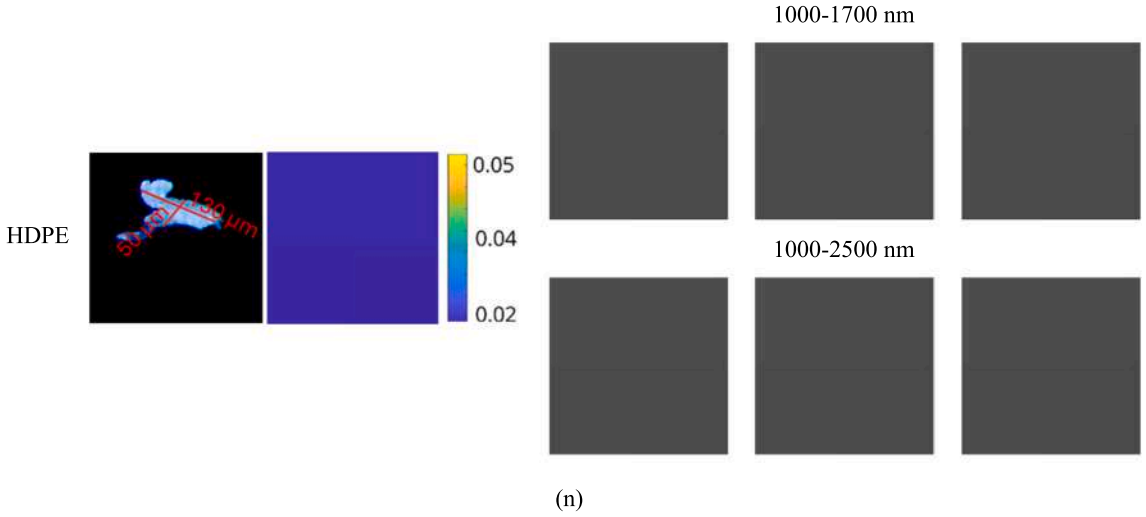

(n)

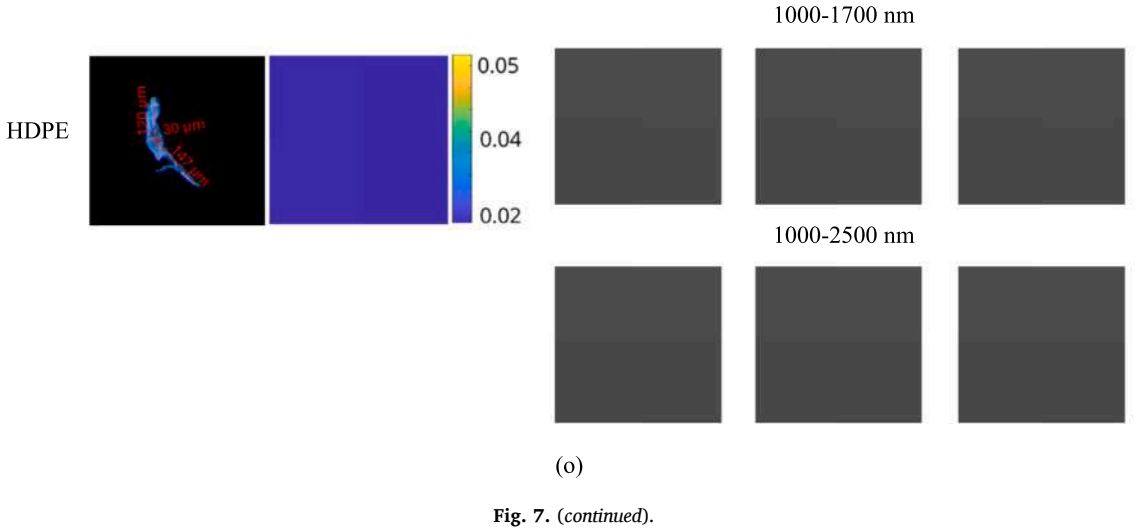

(o)

Fig. 7. (*continued*).

3.2.2. *30 μm/pixel resolution*

At a higher spectral resolution of 30 μm/pixel, the classification results (Fig. 6a and b) are influenced by the increased variability of the spectral signatures due to the three-dimensionality of the particles captured at a higher magnification with a low DOF. In the 1000–1700 nm spectral range (Fig. 6a), PLS-DA misclassifies some pixels among polymer classes in MP particles of PP and HDPE across all the three size classes, as highlighted in green boxes. On the contrary, ECOC-SVM and NNPR show a more accurate polymer classification by leveraging their ability to capture non-linear variance. Moreover, as in the previous case, all models produce a small edge effect, due to the erroneous assignment of MPs pixels to the background class (orange boxes). This effect does not affect the polymer identification in the case of ECOC-SVM and NNPR, whereas for PLS-DA it can contribute to reduce its prediction

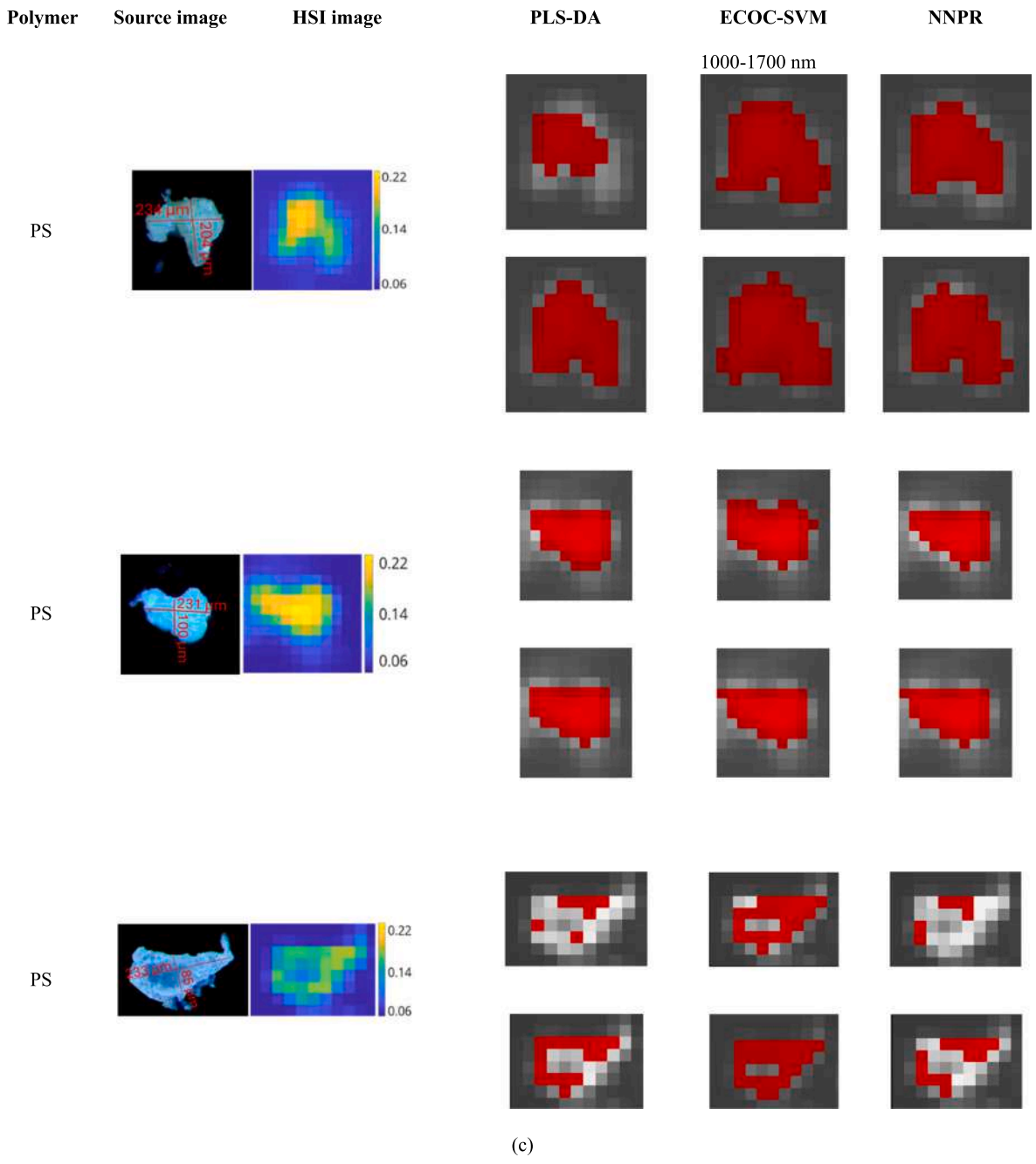

Fig. 8. Source image, hyperspectral image with reflectance color bar and classification results of PLS-DA, ECOC-SVM and NNPR models applied to hyperspectral images of MP particles (PS, PP and HDPE) at resolution of 30 μm/pixel in the 1000–1700 and 1000–2500 nm spectral ranges.

ability when combined with pixels misclassification. For the 1000–2500 nm spectral range (Fig. 6b), misclassified pixels at particle edges (orange boxes) are fewer compared to the 1000–1700 nm range, and they do not significantly reduce the effective recognition of the polymers. Furthermore, predictions are more accurate across all MPs sizes, including those obtained by PLS-DA model. ECOC-SVM provides the most precise classification as evidenced by the particles appearing better defined and closely matching the source image, compared to NNPR and PLS-DA (green boxes).

Performance parameters in Cal and CV (Tables S5 and S6) show that in the 1000–1700 nm spectral range, all classifiers exhibit high-quality results with values ranging from 0.94 to 1.00 for PLS-DA, from 0.97 to 1.00 for ECOC-SVM and from 0.95 to 1.00 for NNPR. However, in the 1000–2500 nm range, PLS-DA shows slightly lower values for (from 0.84 to 1.00), while ECOC-SVM and NNPR maintain high accuracy (both from 0.99 to 1.00). The performance parameters in prediction (Tables S7 and S8) are better in the 1000–2500 nm spectral range than in the 1000–1700 nm for all the classifiers and ECOC-SVM achieves the best parametric performances in both spectral ranges (from 0.87 to 1.00), followed by NNPR (from 0.74 to 1.00) and PLS-DA (from 0.66 to 1.00). The obtained results are in agreement with the findings on the use of SVM techniques for MPs identification on filter papers using HSI (Shan et al., 2019).

These classification results suggest that the 1000–2500 nm spectral range significantly improves parametric performances compared to the 1000–1700 nm range, particularly when using nonlinear classifiers like

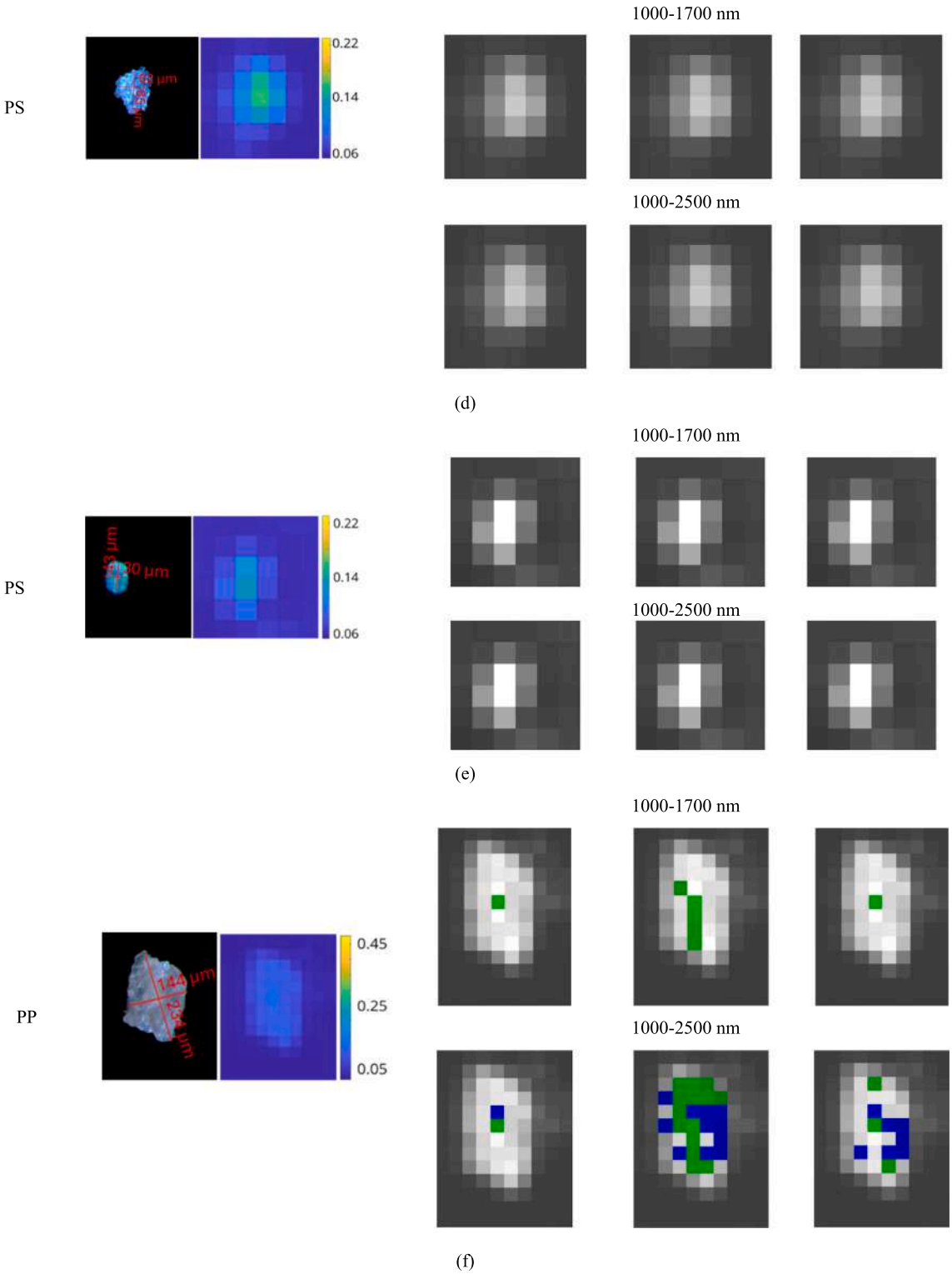

Fig. 8. (*continued*).

ECOC-SVM.). Therefore, hyperspectral images of MPs acquired at this spatial resolution, being more influenced by DOF, can be better processed using a classifier able to capture the non-linear relationship of spectral data, such as ECOC-SVM. It is important to highlight that the model performances can be influenced by several factors, such as the presence of chemical additives, biofilms or physical characteristics such as light scattering as reported by Goyetche et al. (2023), especially at 30 µm/pixel. Such issue can be overcome increasing the spectral library constituting the training dataset.

3.3. Limit of detection (LOD) results

To assess the limit of detection (LOD), hyperspectral images were acquired in the two spatial resolutions and spectral ranges, and classified with the three built models. The prediction maps of single MP particles of the three polymers with a diameter ranging from 30 to 250 µm, with

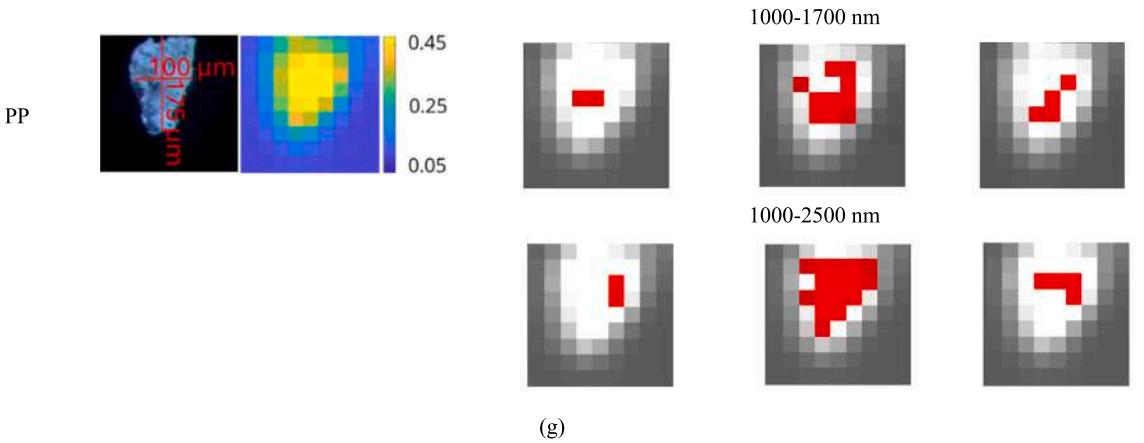
PP
100 µm
75 µm
0.45
0.25
0.05
1000-1700 nm
1000-2500 nm

(g)

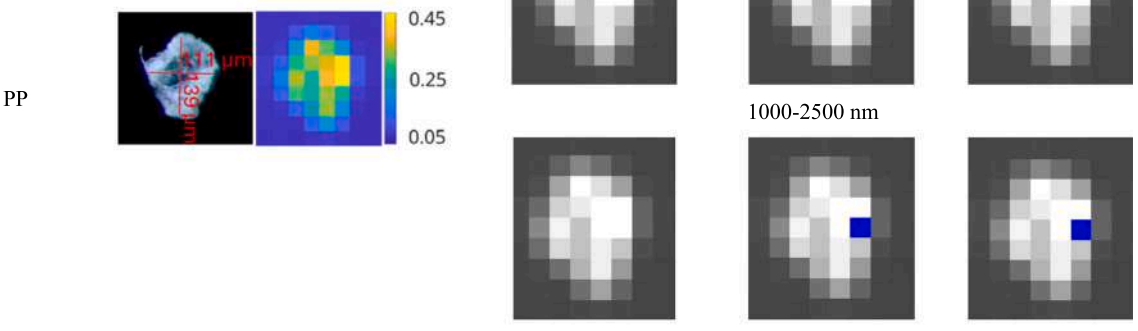
PP
111 µm
139 µm
0.45
0.25
0.05
1000-1700 nm
1000-2500 nm

(h)


PP
32 µm
96 µm
0.45
0.25
0.05
1000-1700 nm
1000-2500 nm

(i)

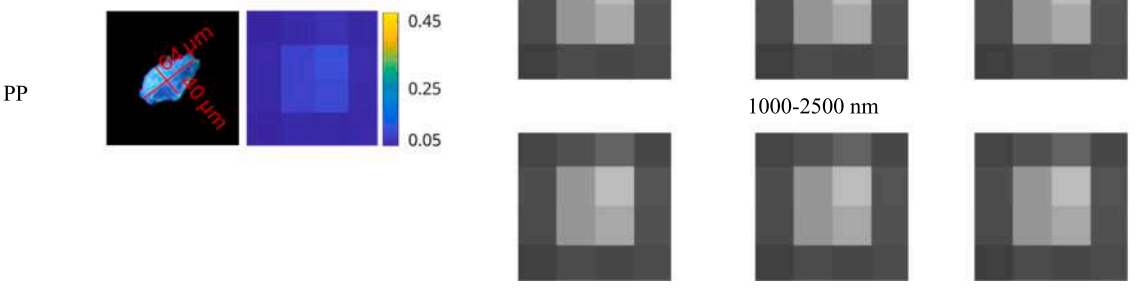
PP
64 µm
40 µm
0.45
0.25
0.05
1000-1700 nm
1000-2500 nm

(j)

Fig. 8. (*continued*).

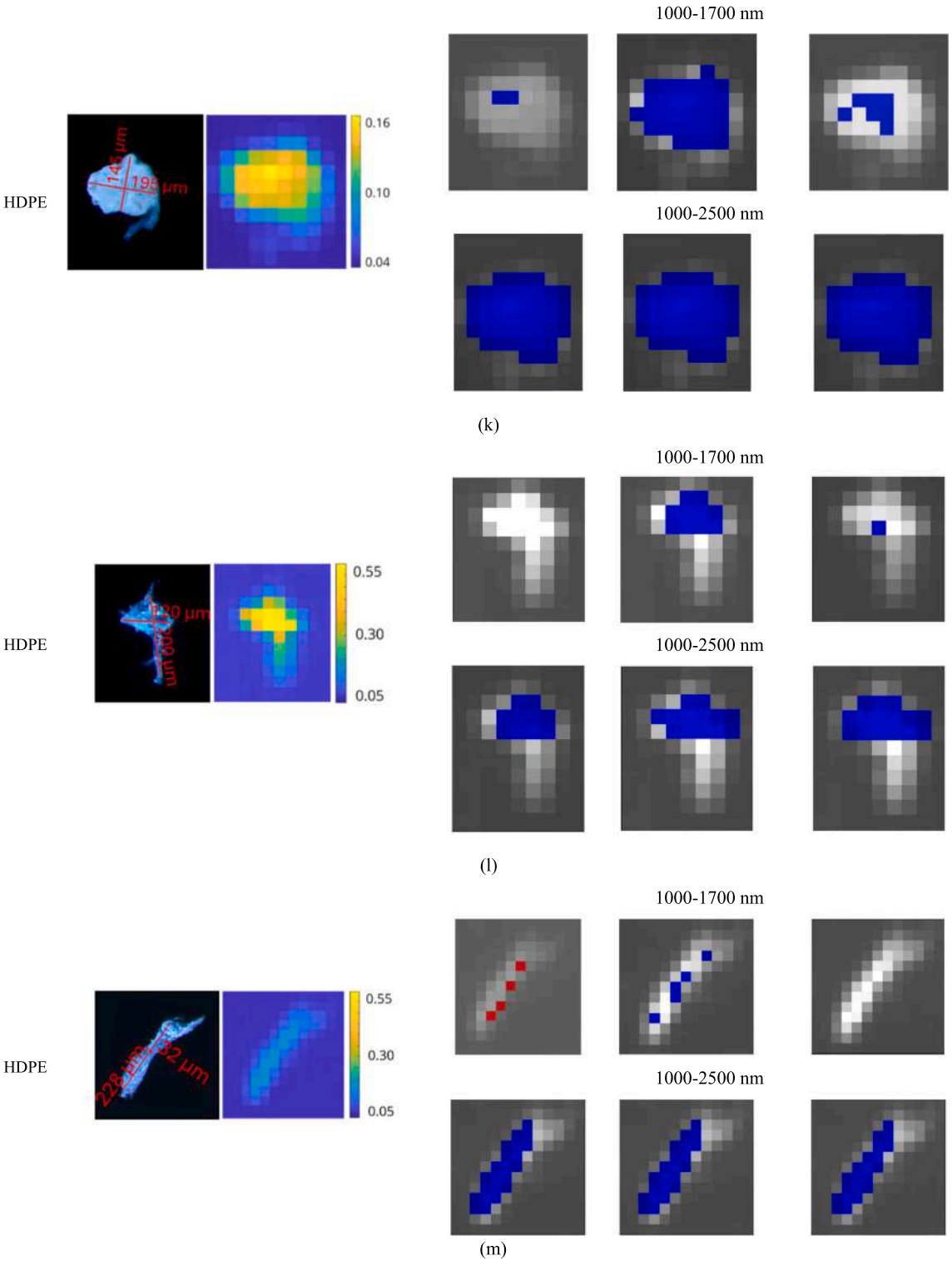

Fig. 8. (*continued*).

reference to the spatial resolution of 150 μm/pixel and 30 μm/pixel are shown in Figs. 7a-o and 8a-o, respectively.

3.3.1. 150 μm/pixel resolution

MP particles with a diameter between 30 and 150 μm are characterized by low reflectance values, similar to those of the background (Fig. 7d, e, h, i, j, n and o) in agreement with what observed in previous studies (Piarulli et al., 2022; Zhu et al., 2021) and are not recognized by any of the classifiers in both spectral ranges, as expected being their size smaller than the spatial resolution.

MP particles with an average diameter between 150 and 250 μm (Fig. 7a, b, c, f, g, k, l and m) also show low reflectance values, but greater than those of background. PLS-DA predictions are incorrect in all cases, while ECOC-SVM and NNPR models in some cases (i.e., Fig. 7a, b,

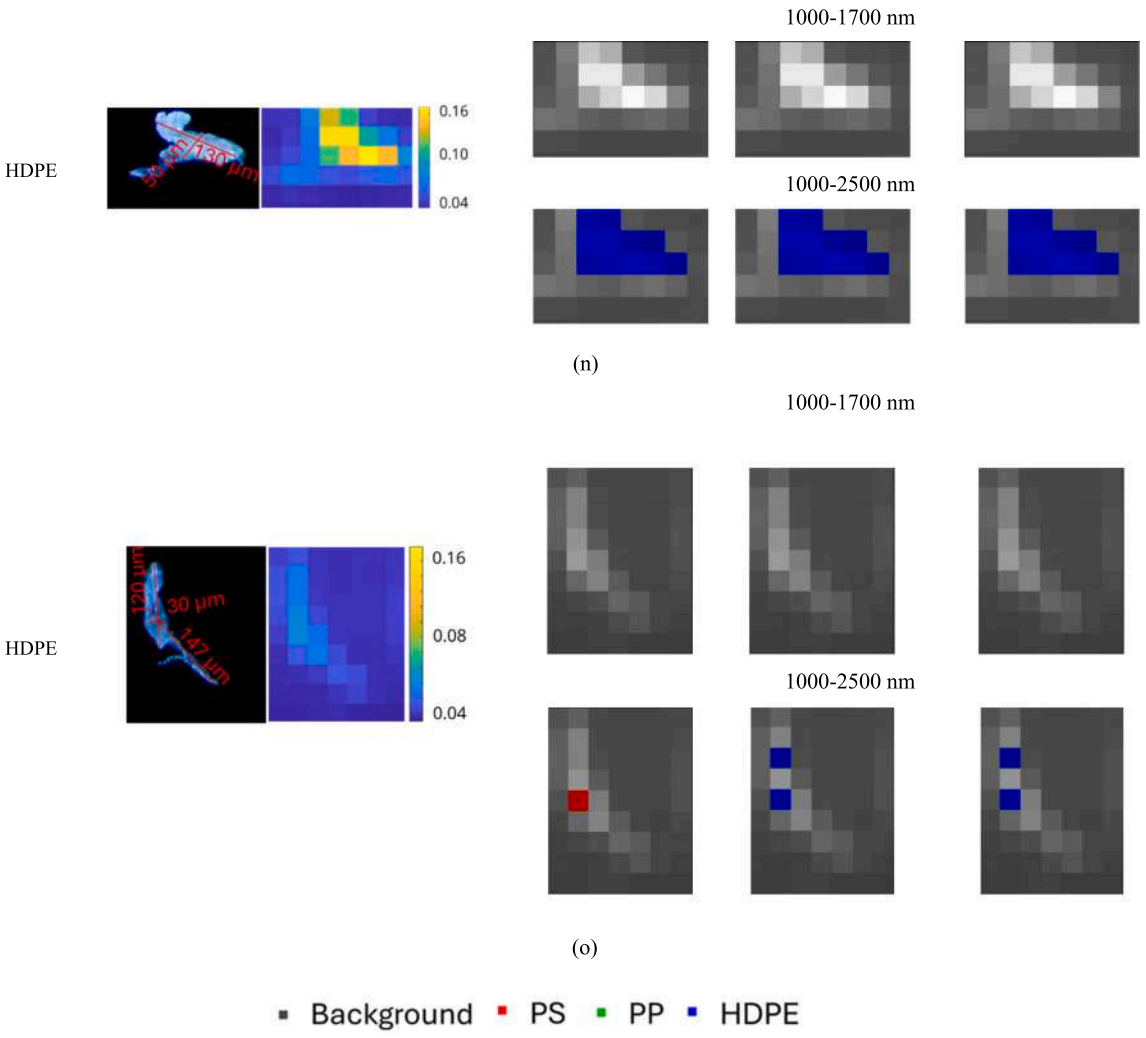

Fig. 8. (*continued*).

c, f, k, l) correctly classify some MP pixels in both spectral ranges. However, these results cannot be considered sufficient for an accurate identification of MPs because such single pixels could be confused with the 'pepper noise effect', observed in paragraph 3.2 for ECOC-SVM and NNPR models at a 150 µm/pixel resolution.

Therefore, for the 150 µm/pixel resolution, the LOD of MP particles can be set at 250 µm, corresponding to the minimum diameter of size class 3, considering that each microplastic has enough pixels to allow an accurate recognition.

3.3.2. 30 µm/pixel resolution

MP particles with a diameter between 30 and 100 µm (Fig. 8d, e, i and j) show very low reflectance values, as already observed in other studies (Piarulli et al., 2022; Zhu et al., 2021), not allowing their distinction from the background by any classifiers, independently from the investigated spectral range.

MP particles with a diameter ranging from 100 to 200 µm (Fig. 8g, h, k, l, n and o) show variable reflectance values, ranging from 0.04 to 0.55. The high variability of reflectance in each single MP particle is due to its three-dimensional structure and thickness, which significantly influences the classification results. Comparing the results in the two spectral ranges, the best performances are obtained in the 1000–2500 nm, with a good classification in most cases for all the three classifiers, as shown in Figs. 8k 8 l, 8n and 8o. On the contrary, in the spectral range 1000–1700 nm the correct recognition of the same MP particles is achieved only by ECOC-SVM model, with the exception of the fragment in Fig. 8n. Finally, the prediction results of MP particles in Fig. 8g and h are not correct as the polymers are misclassified by all models in both spectral ranges.

MPs with a diameter between 200 and 250 µm (Fig. 8a, b, c, f and m) show more homogeneous reflectance values, ranging from 0.10 to 0.22, with lower values along the edge. Looking at each single particle of this size range, the MPs with more uniform reflectance values (Fig. 8a and b) show a correct classification by all the classification models in both the spectral ranges; on the contrary, MPs with higher reflectance variability, due to both the morphological complexity of the particle and its textural features (Fig. 8c, f and m) are better classified by ECOC-SVM, in particular in the range 1000–2500 nm.

Therefore, for the 30 µm/pixel resolution, the LOD of MP particles can be set in the size range of 100–200 µm, acquiring hyperspectral images in the spectral range of 1000–2500 nm and processing data with a nonlinear classification method, like ECOC-SVM, as it is less affected by the noise in the MPs spectrum occurring for the small particle size.

4. Conclusions

In this study, an analytical protocol for classification of MPs by HSI was defined, testing different setups: 1) two spatial resolutions (150 and 30 µm/pixel), 2) two wavelength ranges (1000–1700 and 1000–2500 nm), and 3) three different classification models (i.e., PLS-DA, ECOC-SVM, NNPR). The study focused on the three most common polymers (i.e., PS, PP and HDPE) of MPs usually polluting the environment.

Based on the results, several conclusions can be drawn for the definition of the optimal analytical protocol for MPs classification using HSI.

For larger MPs (>250 μm), the ideal protocol includes a spatial resolution of 150 μm/pixel, a spectral range between 1000 and 1700 nm and PLS-DA as preferred classification model. This setup is efficient in terms of time and cost while maintaining accurate MPs classification. The PLS-DA linear classification model provides comparable performance to nonlinear models but is easier and faster to apply.

In contrast, for smaller MPs (<250 μm), the optimal configuration involves a higher spatial resolution of 30 μm/pixel and a broader spectral range of 1000–2500 nm. In this case, the most suitable classification model is the ECOC-SVM. This configuration enhances parametric performance significantly. The ECOC-SVM model, which captures the nonlinear relationships in spectral data, is better suited for processing hyperspectral images at this higher resolution, offering more accurate classification despite increased DOF influence.

Concerning the LOD for MPs, the 150 μm/pixel resolution offers a detection limit of 250 μm, ensuring that each MP particle at this size has sufficient pixel coverage for accurate recognition. On the other hand, the 30 μm/pixel resolution provides a LOD ranging from 100 to 200 μm. Hyperspectral images acquired within the 1000–2500 nm range and processed using a nonlinear classification method like ECOC-SVM can effectively mitigate noise in the MP spectrum for smaller particles.

In summary, for efficient and cost-effective analysis of MPs larger than 250 μm, it is recommended to use the 150 μm/pixel resolution and 1000–1700 nm spectral range with a linear classification model like PLS-DA. However, for a more detailed analysis of MP particles also in terms of morphological and morphometrical parameters, it is better to use the 30 mm/pixel resolution. For MPs smaller than 250 μm, it is suggested to adopt a higher spatial resolution of 30 μm/pixel and a broader spectral range of 1000–2500 nm, employing a nonlinear model such as ECOC-SVM for improved accuracy in classification.

These conclusions offer a comprehensive guide for selecting the appropriate acquisition conditions and data processing methods to optimize the characterization of MPs of different sizes using HSI.

Funding

The research was carried out in the framework of the Enlarged Partnerships supported under the National Recovery and Resilience Plan (NRRP), Mission 4, Component 2, Investment 1.3 funded by the European Union—NextGenerationEU (RETURN project “Multi-risk science for resilient communities under a changing climate”, no. PE00000005, CUP B53C22004020002.

CRediT authorship contribution statement

Silvia Serranti: Writing – review & editing, Validation, Supervision, Resources, Methodology, Formal analysis, Conceptualization. **Giuseppe Capobianco:** Writing – original draft, Validation, Software, Methodology, Investigation, Formal analysis, Data curation, Conceptualization. **Paola Cucuzza:** Writing – original draft, Validation, Software, Methodology, Investigation, Formal analysis, Data curation. **Giuseppe Bonifazi:** Writing – review & editing, Supervision, Resources.

Declaration of competing interest

The authors declare that they have no known competing financial interests or personal relationships that could have appeared to influence the work reported in this paper.

Data availability

Data will be made available on request.

Appendix A. Supplementary data

Supplementary data to this article can be found online at https://doi.org/10.1016/j.scitotenv.2024.176630.

References

Amigo, J.M., Martí, I., Gowen, A., 2013. Hyperspectral imaging and chemometrics: a perfect combination for the analysis of food structure, composition and quality. In: Data Handling in Science and Technology, vol. 28. Elsevier, pp. 343–370.

Amigo, J.M., Babamoradi, H., Elcoroaristizabal, S., 2015. Hyperspectral image analysis. A tutorial. Anal. Chim. Acta 896, 34–51. https://doi.org/10.1016/j.aca.2015.09.030.

Ballabio, D., Consonni, V., 2013. Classification tools in chemistry. Part 1: linear models. PLS-DA. Analytical methods 5 (16), 3790–3798.

Barker, M., Rayens, W., 2003. Partial least squares for discrimination. J. Chemom. 17, 166–173.

Barnes, R.J., Dhanoa, M.S., Lister, S.J., 1989. Standard normal variate transformation and de-trending of near-infrared diffuse reflectance spectra. Appl. Spectrosc. 43 (5), 772–777.

Beć, K.B., Grabska, J., Badzoka, J., Huck, C.W., 2021. Spectra-structure correlations in NIR region of polymers from quantum chemical calculations. The cases of aromatic ring, C= O, C≡ N and C-Cl functionalities. Spectrochim. Acta A Mol. Biomol. Spectrosc. 262, 120085.

Bonifazi, G., Capobianco, G., Serranti, S., 2018. A hierarchical classification approach for recognition of low-density (LDPE) and high-density polyethylene (HDPE) in mixed plastic waste based on short-wave infrared (SWIR) hyperspectral imaging. Spectrochim. Acta A Mol. Biomol. Spectrosc. 198, 115–122.

Bonifazi, G., Capobianco, G., Cucuzza, P., Serranti, S., Uzzo, A., 2022. Recycling-oriented characterization of the PET waste stream by SWIR hyperspectral imaging and variable selection methods. Detritus 18, 42–49.

Bonifazi, G., Capobianco, G., Serranti, S., 2023. Fast and effective classification of plastic waste by pushbroom hyperspectral sensor coupled with hierarchical modelling and variable selection. Resour. Conserv. Recycl. 197, 107068.

Bro, R., Smilde, A.K., 2003. Centering and scaling in component analysis. J. Chemom. 17 (1), 16–33.

Bro, R., Smilde, A.K., 2014. Principal component analysis. Anal. Methods 6, 2812.

Calvini, R., Ulrici, A., Amigo, J.M., 2019. Growing applications of hyperspectral and multispectral imaging. Data handling in science and technology 32, 605–629.

Cao, F., Yang, Z., Ren, J., Jiang, M., Ling, W.K., 2017. Linear vs. nonlinear extreme learning machine for spectral-spatial classification of hyperspectral images. Sensors 17 (11), 2603.

Chang, H.H., Lin, L.S., Chen, N., 2013. Particle-swarm-optimization-based nonintrusive demand monitoring and load identification in smart meters. IEEE Trans. Ind. Appl. 49 (5), 2229–2236.

Chen, C., Wang, Y., Zhang, N., Zhang, Y., Zhao, Z., 2023. A review of hyperspectral image super-resolution based on deep learning. Remote Sens. 15 (11), 2853.

Cheung, C.K.H., Not, C., 2023. Impacts of extreme weather events on microplastic distribution in coastal environments. Sci. Total Environ. 166723.

Christian, A.E., Köper, I., 2023. Microplastics in biosolids: a review of ecological implications and methods for identification, enumeration, and characterization. Sci. Total Environ. 864, 161083.

Cucuzza, P., Serranti, S., Capobianco, G., Bonifazi, G., 2023. Multi-level color classification of post-consumer plastic packaging flakes by hyperspectral imaging for optimizing the recycling process. Spectrochim. Acta A Mol. Biomol. Spectrosc. 302, 123157.

Datta, D., Mallick, P.K., Bhoi, A.K., Ijaz, M.F., Shafi, J., Choi, J., 2022. Hyperspectral image classification: potentials, challenges, and future directions. Comput. Intell. Neurosci. 2022.

Deng, F., Guo, S., Zhou, R., Chen, J., 2017. Sensor multifault diagnosis with improved support vector machines. IEEE Trans. Autom. Sci. Eng. 14, 1053–1063. https://doi.org/10.1109/TASE.2015.2487523.

Du, J., Xu, S., Zhou, Q., Li, H., Fu, L., Tang, J., Wang, Y., Peng, X., Xu, Y., Du, X., 2020. A review of microplastics in the aquatic environmental: distribution, transport, ecotoxicology, and toxicological mechanisms. Environ. Sci. Pollut. Res. 27, 11494–11505.

Du, R., Sun, X., Lin, H., Pan, Z., 2022. Assessment of manta trawling and two newly-developed surface water microplastic monitoring techniques in the open sea. Sci. Total Environ. 842, 156803.

Duan, Y., Zou, B., Xu, J., Chen, F., Wei, J., Tang, Y.Y., 2021. OAA-SVM-MS: a fast and efficient multi-class classification algorithm. Neurocomputing 454, 448–460. https://doi.org/10.1016/J.NEUCOM.2021.04.115.

Duis, K., Coors, A., 2016. Microplastics in the aquatic and terrestrial environment: sources (with a specific focus on personal care products), fate and effects. Environ. Sci. Eur. 28 (1), 1–25.

Eigenvector, 2018. https://www.wiki.eigenvector.com/index.php?title=Confusionmatrix.

Esquerre, C., Gowen, A.A., Burger, J., Downey, G., O'Donnell, C.P., 2012. Suppressing sample morphology effects in near infrared spectral imaging using chemometric data pre-treatments. Chemom. Intell. Lab. Syst. 117, 129–137.

Faltynkova, A., Wagner, M., 2023. Developing and testing a workflow to identify microplastics using near infrared hyperspectral imaging. Chemosphere 139186.

Faltynkova, A., Johnsen, G., Wagner, M., 2021. Hyperspectral imaging as an emerging tool to analyze microplastics: a systematic review and recommendations for future development. Microplastics and Nanoplastics 1 (1), 1–19.
Fiore, L., Serranti, S., Mazziotti, C., Riccardi, E., Benzi, M., Bonifazi, G., 2022. Classification and distribution of freshwater microplastics along the Italian Po river by hyperspectral imaging. Environ. Sci. Pollut. Res. 29 (32), 48588–48606.
Gewali, U.B., Monteiro, S.T., Saber, E.. Machine Learning Based Hyperspectral Image Analysis. arXiv:1802.08701.
Goyetche, R., Kortazar, L., Amigo, J.M., 2023. Issues with the detection and classification of microplastics in marine sediments with chemical imaging and machine learning. TrAC Trends Anal. Chem. 117221.
Hale, R.C., Seeley, M.E., La Guardia, M.J., Mai, L., Zeng, E.Y., 2020. A global perspective on microplastics. J. Geophys. Res. Oceans 125 (1), e2018JC014719.
Hu, W., Huang, Y., Wei, L., Zhang, F., Li, H., 2015. Deep convolutional neural networks for hyperspectral image classification. J Sens 1–12.
Huang, Z., Hu, B., Wang, H., 2023. Analytical methods for microplastics in the environment: a review. Environ. Chem. Lett. 21 (1), 383–401.
Issac, M.N., Kandasubramanian, B., 2021. Effect of microplastics in water and aquatic systems. Environ. Sci. Pollut. Res. 28, 19544–19562.
Jolliffe, I.T., 1986. Principal Component Analysis: With 26 Illustrations. Springer.
Jolliffe, I.T., 2002. Principal Component Analysis. Springer, New York, NY.
Kavya, A.N.L., Sundarrajan, S., Ramakrishna, S., 2020. Identification and characterization of micro-plastics in the marine environment: a mini review. Mar. Pollut. Bull. 160, 111704.
Lee, H., Kim, S., Sin, A., Kim, G., Khan, S., Nadagouda, M.N., Sahle-Demessie, E., Han, C., 2023. Pretreatment methods for monitoring microplastics in soil and freshwater sediment samples: a comprehensive review. Sci. Total Environ. 871, 161718.
Li, F., Wang, Y.K., Zhu, L., 2014. Research on noninvasive risk evaluation of diabetes mellitus based on neural network pattern recognition. Spectrosc. Spectr. Anal. 34 (5), 1327–1331.
Liu, Z., You, X.Y., 2023. Recent progress of microplastic toxicity on human exposure based on in vitro and in vivo studies. Sci. Total Environ. 166766.
Lodhi, V., Chakravarty, D., Mitra, P., 2019. Hyperspectral imaging system: development aspects and recent trends. Sensing and Imaging 20, 1–24.
Miller, C.E., 1991. Near-infrared spectroscopy of synthetic polymers. Appl. Spectrosc. Rev. 26 (4), 277–339.
Mishra, P., Nordon, A., Tschannerl, J., Lian, G., Redfern, S., Marshall, S., 2018. Near-infrared hyperspectral imaging for non-destructive classification of commercial tea products. J. Food Eng. 238, 70–77.
Munoz-Pineiro, M., 2018. Microplastics: Focus on Food and Health, EUR N/A. Publications Office of the European Union, Luxembourg. ISBN N/A, JRC110629.
Ozdemir, A., Polat, K., 2020. Deep learning applications for hyperspectral imaging: a systematic review. Journal of the Institute of Electronics and Computer 2 (1), 39–56.
Piarulli, S., Malegori, C., Grasselli, F., Airoldi, L., Prati, S., Mazzeo, R., Sciutto, G., Oliveri, P., 2022. An effective strategy for the monitoring of microplastics in complex aquatic matrices: exploiting the potential of near infrared hyperspectral imaging (NIR-HSI). Chemosphere 286, 131861.
Ragusa, A., Svelato, A., Santacroce, C., Catalano, P., Notarstefano, V., Carnevali, O., Papa, F., Rongioletti, M.C.A., Baiocco, F., Draghi, S., D'Amore, E., Rinaldo, D., Matta, M., Giorgini, E., 2021. Plasticenta: first evidence of microplastics in human placenta. Environ. Int. 146, 106274.
Rani-Borges, B., Gomes, E., Maricato, G., de Carvalho Lins, L.H.F., de Moraes, B.R., Lima, G.V., Cortes, L., G, F., Tavares, M., Pereira, P.H.C., Ando, R.A., Queiroz, L.G., 2023. Unveiling the hidden threat of microplastics to coral reefs in remote South Atlantic islands. Sci. Total Environ. 897, 165401.
Rinnan, Å., van den Berg, F., Engelsen, S.B., 2009. Review of the most common preprocessing techniques for near-infrared spectra. TrAC - Trends Anal. Chem. 28, 1201–1222.
Rytelewska, S., Dąbrowska, A., 2022. The Raman spectroscopy approach to different freshwater microplastics and quantitative characterization of polyethylene aged in the environment. Microplastics 1 (2), 263–281.
Savitzky, A., Golay, M.J., 1964. Smoothing and differentiation of data by simplified least squares procedures. Anal. Chem. 36 (8), 1627–1639.
Schmidt, L.K., Bochow, M., Imhof, H.K., Oswald, S.E., 2018. Multi-temporal surveys for microplastic particles enabled by a novel and fast application of SWIR imaging spectroscopy–study of an urban watercourse traversing the city of Berlin, Germany. Environ. Pollut. 239, 579–589.
Serranti, S., Gargiulo, A., Bonifazi, G., 2012. Classification of polyolefins from building and construction waste using NIR hyperspectral imaging system. Resour. Conserv. Recycl. 61, 52–58.
Serranti, S., Palmieri, R., Bonifazi, G., Cózar, A., 2018. Characterization of microplastic litter from oceans by an innovative approach based on hyperspectral imaging. Waste Manag. 76, 117–125.
Serranti, S., Fiore, L., Bonifazi, G., Takeshima, A., Takeuchi, H., Kashiwada, S., 2019, November. Microplastics characterization by hyperspectral imaging in the SWIR range. In: SPIE Future Sensing Technologies, vol. 11197. SPIE, pp. 134–140.
Serranti, S., Cucuzza, P., Bonifazi, G., 2020. Hyperspectral imaging for VIS-SWIR classification of post-consumer plastic packaging products by polymer and color. In: SPIE Future Sensing Technologies, vol. 11525. SPIE, pp. 212–217.
Shan, J., Zhao, J., Zhang, Y., Liu, L., Wu, F., Wang, X., 2019. Simple and rapid detection of microplastics in seawater using hyperspectral imaging technology. Anal. Chim. Acta 1050, 161–168.
Tasseron, P., van Emmerik, T., Peller, J., Schreyers, L., Biermann, L., 2021. Advancing floating macroplastic detection from space using experimental hyperspectral imagery. Remote Sens. 13, 2335.
Vethaak, A.D., Legler, J., 2021. Microplastics and human health. Science 371 (6530), 672–674.
Vidal, M., Amigo, J.M., 2012. Preprocessing of hyperspectral images. Essential steps before image analysis. Chemom. Intell. Lab. Syst. 117, 138–148.
Vidal, C., Pasquini, C., 2021. A comprehensive and fast microplastics identification based on near-infrared hyperspectral imaging (HSI-NIR) and chemometrics. Environ. Pollut. 285, 117251.
Vidal, M., Gowen, A., Amigo, J.M., 2012. NIR hyperspectral imaging for plastics classification. NIR News 23, 13–15.
Welsh, B., Aherne, J., Paterson, A.M., Yao, H., McConnell, C., 2022. Atmospheric deposition of anthropogenic particles and microplastics in south-Central Ontario, Canada. Sci. Total Environ. 835, 155426. https://doi.org/10.1016/j.scitotenv.2022.155426.
Weyer, L., 2007. Practical Guide to Interpretive Near-Infrared Spectroscopy. CRC Press. https://doi.org/10.1002/anie.200885575.
Workman, J., Weyer, L., 2012. Practical Guide and Spectral Atlas for Interpretive Near-Infrared. CRC. https://doi.org/10.1201/b11894.
Yang, L., Zhang, Y., Kang, S., Wang, Z., Wu, C., 2021. Microplastics in soil: A review of methods, occurrence, sources, and potential risk. Sci. Total Environ. 780, 146546.
Zarfl, C., 2019. Promising Techniques and Open Challenges for identification and quantification of microplastics in environmental matrices. Anal. Bioanal. Chem. 411, 3743–3756.
Zhou, C., Liu, S., Liu, P., 2016, July. Neural network pattern recognition based non-intrusive load monitoring for a residential energy management system. In: 2016 3rd International Conference on Information Science and Control Engineering (ICISCE). IEEE, pp. 483–487.
Zhu, C., Kanaya, Y., Nakajima, R., Tsuchiya, M., Nomaki, H., Kitahashi, T., Fujikura, K., 2020. Characterization of microplastics on filter substrates based on hyperspectral imaging: laboratory assessments. Environ. Pollut. 263, 114296.
Zhu, C., Kanaya, Y., Tsuchiya, M., Nakajima, R., Nomaki, H., Kitahashi, T., Fujikura, K., 2021. Optimization of a hyperspectral imaging system for rapid detection of microplastics down to 100 μm. MethodsX 8, 101175.